CZECH TECHNICAL UNIVERSITY IN PRAGUE

FACULTY OF MECHANICAL ENGINEERING

MASTER OF SCIENCE – PROCESS ENGINEERING

CFD SIMULATION OF HYDRODYNAMIC CONDITIONS IN FLAT PANEL PHOTOBIOREACTOR

SUPERVISOR

Ing. Mgr. Vojtěch Bělohlav

AUTHOR

Davide Roletto

ACADEMIC YEAR 2020 – 2021

MASTER'S THESIS ASSIGNMENT

I. Personal and study details

Student's name: **Roletto Davide** Personal ID number: **491106**

Faculty / Institute: **Faculty of Mechanical Engineering**

Department / Institute: **Department of Process Engineering**

Study program: **Mechanical Engineering**

Branch of study: **Process Engineering**

II. Master's thesis details

Master's thesis title in English:

CFD simulation of hydrodynamic conditions in flat panel photobioreactor

Master's thesis title in Czech:

CFD simulace hydrodynamických podmínek v deskovém fotobioreaktoru

Guidelines:

Design the element for homogenization of culture medium in pilot-plant flat panel photobioreactor. Prepare a literature and patent review of existing design variants for mixing and homogenization of the microalgal culture medium. Based on the critical review, design the most suitable element for a pilot-plant flat panel photobioreactor. Prepare drawing documentation and a 3D model of the element for homogenization. For the selected variant, elaborate a CFD model to simulate hydrodynamic conditions. Based on the created model, evaluate the influence of the designed element on the operating conditions of the pilot-plant flat panel photobioreactor.

Bibliography / sources:

According to the recommendation of Thesis supervisor

Name and workplace of master's thesis supervisor:

Ing. Mgr. Vojtěch Bělohlav, Department of Process Engineering, FME

Name and workplace of second master's thesis supervisor or consultant:

Date of master's thesis assignment: **21.04.2021** Deadline for master's thesis submission: **04.06.2021**

Assignment valid until: **19.09.2021**

Ing. Mgr. Vojtěch Bělohlav	prof. Ing. Tomáš Jirout, Ph.D.	prof. Ing. Michael Valášek, DrSc.
Supervisor's signature	Head of department's signature	Dean's signature

III. Assignment receipt

The student acknowledges that the master's thesis is an individual work. The student must produce his thesis without the assistance of others, with the exception of provided consultations. Within the master's thesis, the author must state the names of consultants and include a list of references.

. | Date of assignment receipt

Student's signature

I confirm that this diploma's work was disposed by myself and independently, under leading of my thesis supervisor. I stated all sources of the documents and literature.

In Prague _____ Davide Roletto

_____

ACKNOWLEDGEMENTS

I would like to acknowledge my supervisor, Ing. Msgr. Vojtěch Bělohlav, for his availability and interest. Thank you for the time and professionalism you have dedicated to me.

I also owe a big debt to the city of Prague, which welcomed me two years ago and offered me wonderful opportunities to study, work and also great friendships.

Today the great satisfaction recompenses all the efforts made. Every single small step brought me to the end of this journey and the beginning of the next one. But I didn't do it all by myself.

Firstly, I want to thank my family. You have been with me all these years, and you have always been willing to support and encourage me when I needed it most. And you have always succeeded.

I am also thankful to all my friends, fundamental elements in such a different historical moment, characterized by distance. We have always found a way to be together, even if we were far away.

And finally, thanks to everyone who believed in me, I hope I have given you a little satisfaction.

Thank you.

Davide

ANNOTATION SHEET

Name: Davide
Surname: Roletto

Title Czech:

CFD simulace hydrodynamických podmínek v deskovém fotobioreaktoru.

Title English:

CFD simulation of hydrodynamic conditions in flat panel photobioreactor.

Scope of work: number of pages: 69
number of figures: 43
number of tables: 10
number of appendices: 1

Academic year: 2020/2021
Language: English
Department: Process Engineering
Specialization: Process Engineering
Supervisor: Ing. Mgr. Vojtěch Bělohlav
Reviewer:

Submitter:

Czech Technical University in Prague. Faculty of Mechanical Engineering, Department of Process Engineering.

Annotation - Czech:

Navrhněte konstrukci vestavby deskového fotobioreaktoru pro homogenizaci proudu kultivačního média. Zpracujte literární a patentovou rešerši existujících konstrukčních variant pro promíchávání a homogenizaci kultivačního média. Na základě kritické rešerše navrhněte nejvhodnějších konstrukci pro poloprovozní deskový fotobioreaktor. Vypracujte výkresovou dokumentaci a 3D model vestavby. Pro navrženou variantu vypracujte CFD model pro simulaci hydrodynamických podmínek. Na základě vytvořeného modelu vyhodnoťte vliv navržené vestavby na provozní podmínky deskového fotobioreaktoru.

Annotation - English:

Design the element for homogenization of culture medium in flat panel photobioreactor. Prepare a literature and patent review of existing design variants for mixing and homogenization of the culture medium. Based on the critical review, design the most suitable constructions for a pilot-plant flat panel photobioreactor. Prepare drawing documentation and a 3D model of the element for homogenization. For the selected variant, elaborate a CFD model to simulate hydrodynamic conditions. Based on the created model, evaluate the influence of the designed element on the operating conditions of the pilot-plant flat panel photobioreactor.

Keywords: Microalgae, Flat panel PBR, Static Mixer, CFD

Utilization:

For Department of Process Engineering, Czech Technical University in Prague

ABSTRACT

Microalgae are an interesting biological source of high-value products. A raw material increasingly used in countless sectors from the food industry to energy production. One of the most critical factors related to microalgae growth is, together with light, mixing: improving the culture homogeneity allows a better distribution of nutrients and ensures the proper exposure of each microorganism to the light.

This research focuses on improving microalgae growth, acting on the hydrodynamical conditions inside a flat panel photobioreactor (PBR) by a novel static mixing system capable of maximizing the exchange of light, avoiding sedimentation, and ensuring a perfect homogenization.

The study has been mainly conducted by CFD analysis. The analysis of the flow has been useful from the design phase to the study of the real effectiveness of this system.

For the study of the flow with CFD analysis, it was created a “virtual” model of the flat panel PBR, and volume rendering, streamlines, and vector plots have been used to visualize the movement inside the flat panel and vortex core region to visualize regions of high energy concentration as vorticity and swirl strength.

The effects of the designed mixing system have been compared with the standard empty chamber also through injection of a tracer. The tracer mass fraction was monitored by defined control points into the chamber, detecting the residence time and the homogenization time.

INTRODUCTION

Microalgae are unicellular microscopic organisms that represent a fascinating source of high-value biological compounds such as polysaccharides, proteins/enzymes, fatty acids, sterols, pigments, vitamins, alkaloids, amino acids, antioxidants, and toxins [1].

These bioactive compounds have positive and essential properties for most living beings. This translates into several applications in numerous industrial sectors from pharmaceutical, cosmetic to food and chemical industries. Microalgae are also considered a third-generation energy source, and they can be used to purify wastewater [2].

Microalgae are, therefore, an interesting starting point for obtaining these natural compounds. However, real-world applications are still expensive, but they can be improved by modifying the production and extraction process [2]. The process of microalgae production is affected by several operating parameters, such as the proper temperature of the culture medium, nutrients utilization or incident light radiation. All these parameters are influenced by the mixing conditions of the culture. Mixing can provide appropriate conditions for uniform distribution of nutrients, avoid temperature gradients, and intensify the utilization of incident light. Moreover, mixing can eliminate the sedimentation of produced microalgae cells. These properties are significant for large scale cultivation systems. Therefore, the study of hydrodynamic conditions is important during the scaling-up of cultivation systems.

This thesis aims to analyze the hydrodynamic conditions within a flat panel Photobioreactor (PBR), one of the best microalgae cultivation systems (on a small to medium scale) to produce microalgae biomass.

To intensify the mixing conditions and homogenize the culture medium flow, the aim is to design an inclined perforated plate (IPP) system. This mixing system

should reduce mounting space/occupied surface to maximize light transmission, and low production cost, thanks to its simple geometry. The IPP system should allow a non-aggressive mixing, which guarantees less energy dissipation and does not damage the microalgae cells. Lastly, the arrangement of the plates should be able to avoid sedimentation during the entire operations, significantly reducing maintenance time.

A stable mathematical model can be a proper tool to evaluate the efficiency of the given mixer geometry. This model can be used as a quantitative representation of a natural phenomenon, its purpose is to represent the phenomenon, in as much detail as possible.

CFD analysis can be useful to understand which parameters are more critical to optimize the geometry of the static mixer, during the design phase, before building the prototypes, saving time and money. This work aims to optimize thy hydrodynamic conditions by installing an internal element that can intensify the mixing and provide a homogenous flow of culture medium. The proper design of the internal element was selected based on the CFD simulation, and thanks the directly comparison with the hydrodynamics in a standard empty flat panel photobioreactor chamber.

TABLE OF CONTENTS

LIST OF FIGURES

LIST OF TABLES

Chapter 1
MICROALGAE

Microalgae, also known as phytoplankton, are single-celled microscopic organisms that live singly or in colonies, in fresh and salt water where they are the most important components in the food chains in these aquatic ecosystems [1]. They are organisms with extraordinary adaptability. They can survive in an environmental context different from the original one. The biodiversity of microalgae is enormous. The existing species are approximately between 200,000 and 800,000 [3].

Microalgae biomass is a rich source of biologically active compounds, such as polysaccharides, proteins/enzymes, fatty acids, sterols, pigments, vitamins, alkaloids, amino acids, antioxidants, and toxins [4].

In Fig. 1 are represented and here briefly explained, six of the most famous microalgae on the market (from left) [5]:

Spirulina is the best-known algae as food and feeds supplement, and it has been the most cultivated algae since the 1970s. There are large farms in the China, USA, India, and other countries, and many small village scales in Europe, Africa, and Asia [6].

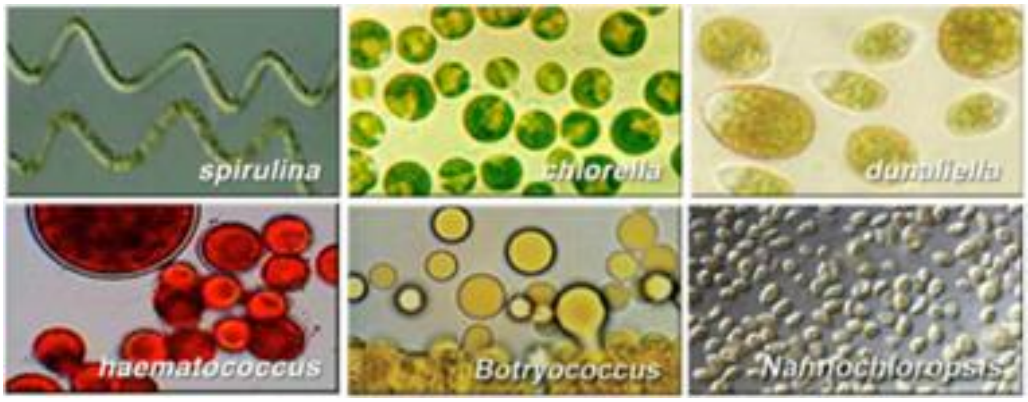

Figure 1 - Microscopic portraits of six commercial microalgae [7].

In 1970, ***Chlorella*** was the first microalgae to be commercially cultivated and sold as a food supplement.

Dunaliella succeeds in water even saltier than the ocean. Too salty to be eaten as a whole food, its beta carotene is extracted as an oil or powder and sold as a food supplement, antioxidant, and pigment for aquaculture feeds [7].

Haematococcus is grown in outdoor ponds and closed systems for carotenoid pigment, extracted as a fish feed supplement to colour salmon flesh and as a human anti-oxidant food supplement.

Botryococcus braunii and ***Nannochloropsis*** are both used for biofuel and nutritional omega-3 oil production.

Around the world, microalgae are currently used in the pharmaceutical, nutraceutical, cosmetic and food industries as natural medicines, food additives and UV protective agents [1], as shown in Fig. 2.

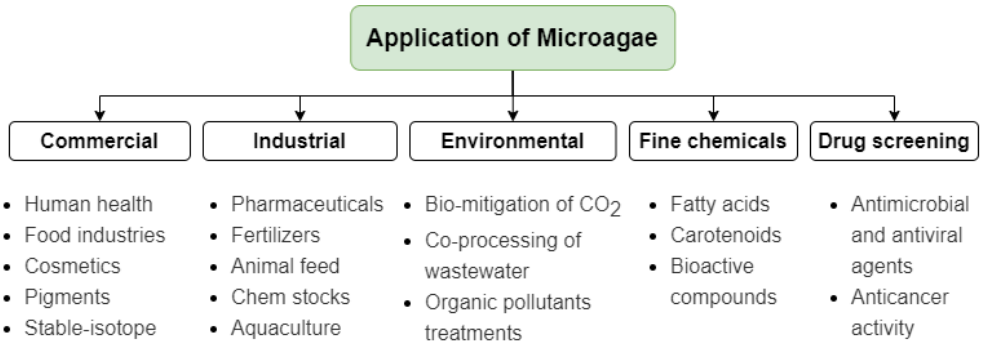

Figure 2 - Applications of microalgae divided by sector [8].

Microalgae are cultivated in all-scale systems, each producing a few tens to several hundred tons of biomass annually. The total global production of commercial microalgal biomass is estimated to be around 10000 tons per year. Almost all commercial production is carried out with open ponds [9].

Microalgae are, therefore, an interesting starting point for obtaining these natural compounds. A future aim is to optimize algal biomass cultivation techniques and encourage research in this field to increase biofuels, hydrogen, and methane production with a sustainable approach. For the harvesting of microalgae, considered a third-generation energy resource, there is also a tendency to use them

to purify wastewater [10]. Many microalgae species can effectively grow in wastewater conditions through their ability to utilize abundant nitrogen and phosphorus present in the wastewater of agricultural or civil origin.

1.1 High-value products

Most microalgae species have a protein content greater than 50% of their dry weight, and some of these proteins, in addition to having lipid-lowering and hypoglycemic properties, can reduce cholesterol and triglyceride levels, so they are typically used for the production of food against obesity [11]. There are species of microalgae capable of producing so-called antifreeze proteins (AFPs). AFP extracts from algae can be used for cryopreservation and storage of frozen foods [12].

Microalgae also produce high amounts of lipids, including ω-3 and ω-6 fatty acids. Among the ω-6 fatty acids, we have gamma-linolenic acid (GLA), important for therapeutic applications and for the formulation of cosmetics. Together with linoleic acid, GLA is considered an essential nutrient, useful for processes related to tissue regeneration. Among the most important ω-3 acids we have instead eicosapentaenoic acid (EPA) and docosahexaenoic acid (DHA) [13]. They are associated with the reduction of cardiovascular problems, arthritis, and hypertension. DHA acid also helps in the functioning of the nervous system.

In terms of pigments, microalgae synthesize compounds belonging to three different classes (chlorophylls, carotenoids, and phycobiliproteins). The primary application of microalgae pigments, in particular β-carotene and astaxanthin, is expressed in the production of food dyes [11].

In addition to vitamin A, microalgae are rich in vitamins C, E, K, thiamine, pyridoxine, riboflavin, niacin, biotin, and tocopherol [4]. These compounds strengthen the immune system and they are essential for various chemical reactions in our bodies. They also regulate the functioning of the nervous system and the growth of tissues and cells. Some vitamins also have an antioxidant function, and others cause blood clotting.

In conclusion, these bioactive compounds have positive and essential properties for most living creatures.

1.2 Microalgal biofuels

1.2.1 Energy crisis

The exponential growth of the human population, rapid industrialization, and better living conditions have led to a constant increase in energy demands. Fossil fuels will no longer be accessible at low cost, and their reckless use is devastating to the environment through the greenhouse effect and the consequent global warming [9].

The related climatic change projections will have significant consequences for both human systems and nature, which determine no more sustainable use of fossil fuels, not only in relation to the quality of the resources, but also on the pollution generated by any type of processes mainly characterized by CO2 emissions.

In Fig. 3, the forecast from Energy Information Administration (EIA) projects that world energy consumption will grow by 50% between 2018 and 2050. The development of emergent countries, such as China and India, is expected to lead the world energy consumption with the consequent increase in the concentration of CO2 in the atmosphere, acidification of the water and loss of biodiversity.

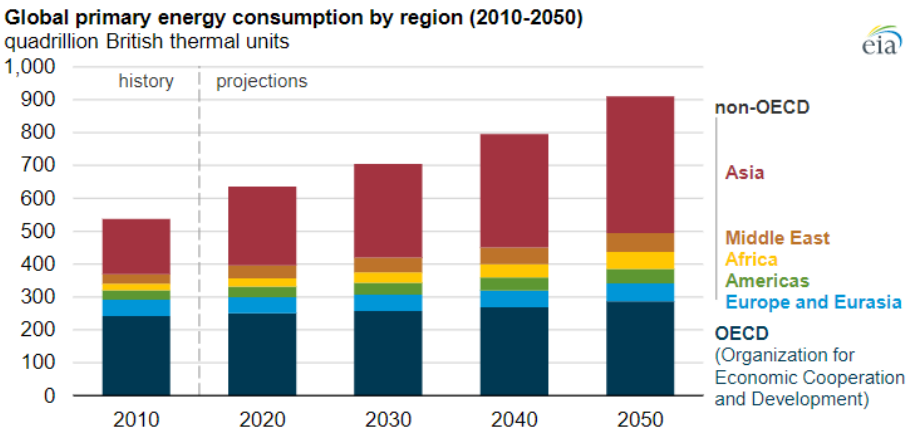

Figure 3 - EIA, International Energy Outlook 2019 [9].

It's becoming clear how much the integration and subsequent replacement of fossil fuels is necessary to cope with the energy demand and meet a sustainable model.

The industrial and transportation sectors together will lead the energy consumption to reach nearly 30% more. Each sector has its favourite fuel. Global liquid fuels consumption will increase more than 20% between 2018 and 2050. Among the different energy sectors, the production of liquid fuels is critical due to the high

dependence on fossil sources; therefore, it would be advisable to carry out, at least, a partial replacement of fossil fuels with biofuels. The focus is shifting to third-generation biofuels [14]; they are on the way to become commercial competitive, and they could become the first substitute of liquid fossil fuel.

1.2.2 Biofuels

Fuels produced from young organic material such as plants (i.e. energy crops) or agricultural, industrial, and household waste. Organic resources or biomass use photosynthesis to stock energy inside by the process of biological carbon fixation in which CO_2 is converted into sugar [10].

When the biomass used in biofuel production can quickly grow back, the fuel is generally considered a renewable form of energy. Moreover, they often have a positive emissions balance, i.e. biofuels are carbon-neutral because, in their growth phase, they can absorb the emissions generated during their combustion (and the energy used during all the processing phases).

This, in fact, is the main difference with fossil fuels, which deriving from older and slower geological processes, they are an exhaustible resource, and above all, they can no more absorb CO_2, and therefore, a priori, they have a negative balance.

Biofuels are usually divided into four categories [15]:

- **1st generation** biofuels are fuels obtained from food crops grown on arable land. The sugar, starch, or oil content of the crop is converted into biodiesel or ethanol. The controversial aspect of this “generation” is selecting land for food or fuel. And usually, fuel has more margin profit.

- **2nd generation** biofuels are fuels obtained from lignocellulosic or woody biomass or agricultural residues/waste. The raw materials used to produce fuels don’t grow on arable land but are byproducts of the primary culture, or they grow on marginal lands. The second-generation raw materials include straw, used vegetable oils, bagasse, municipal, industrial, and food solid waste.

- **3rd generation** biofuels derive from unicellular algae, which can fix carbon atoms from the air's carbon dioxide thanks to photosynthesis. The fixed CO2 is used to synthesize lipids and other cellular components. These lipids can then be extracted and trans-esterified into biodiesel.

- **4th generation** biofuels are based on the modification of the genome of some microorganisms to transform water, sugar, and carbon dioxide directly into biofuels. All this without using any type of plant biomass and subsequent chemical or biological modifications necessary for the biofuels of the previous manufacture.

Microalgae as feedstock:

Microalgae are one of the most interesting natural sources in the world. They contribute to approximately 50% of global photo-synthetic activity. For autotrophic algae, photosynthesis is a key component of their survival, whereby they convert solar radiation and CO_2 absorbed by chloroplasts in energy to support their growth [8].

Table 1 shows the great potential of microalgae as a feedstock source and why using 3rd generation fuels can solve the land use problems [10].

Feedstock source	**Lipid content** *(% oil/s.s.)*	**Oil yield** *(L oil/ha)*	**Yield in biodiesel** *(kg biodiesel/ha)*
Soya	18	446 - 635	*562*
Jatropha	28	741 - 1.890	*656*
Carmelina	42	915	*809*
Palm oil	36	5 500	*4 750*
Microalgae (low content of oil)	30	58 700	*51 930*
Microalgae (medium content of oil)	50	97 800	*86 515*
Microalgae (high content of oil)	*70*	*136 900*	*121 105*

Table 1 - Comparison between food crop and algae biomass [16].

Concerning the oil yield, microalgae show higher values than other oil crops. Table 1 compares the production and land use efficiencies for the biodiesel produced by microalgae and other oil crops. It is evident that microalgae are the most

advantageous both in terms of oil yield and for the high biodiesel productivity (from 52000 to 120000 kg of biodiesel/ha) and at the same time require a smaller extension of lands (even 49-132 times less than the land required for the cultivation of rapeseed and soybeans).

Microalgae, as explained before, can be particularly useful to reduce the concentration of inorganic nitrogen and phosphorus in wastewater [10].

1.3 Photosynthesis

The photosynthetic activity of microalgae is fundamental for life on earth; it is estimated that they produce 50% of atmospheric oxygen while simultaneously absorbing carbon dioxide [17], the main greenhouse gas for the growth and synthesis of new organic matter. To produce 1 kg of microalgal biomass is required 1,8 kg of CO_2 [18].

Microalgae are photosynthetic organisms that are more efficient in the conversion of solar energy than common plants. Since living in fresh or salt water, they have a large availability of carbon dioxide and nutrients [17]. Organic molecules are synthesized from dissolved inorganic substances during the photosynthesis process, using solar radiation as an energy source [19]. The general reaction of photosynthesis is as follows:

$$6\,CO_2 + 6\,H_2O + Light \rightarrow C_6H_{12}O_6 + 6\,O_2 \quad (1)$$

The photosynthetic process takes place into chloroplasts and occurs mainly in two stages [19]:

The **light phase** can only occur with the presence of light and converts solar energy into chemical energy; its main products are ATP (Adenosine triphosphate) and reducing compounds NADPH (Nicotinamide adenine dinucleotide phosphate). In this phase, molecular oxygen is released.

The **dark phase** is light independent, and thanks to the molecules produced during the light phase, carbon dioxide is organized into sugars.

1.4 Production process

The whole process of microalgae production can be divided into two phases, as shown in Fig. 4. The upstream process includes cultivation techniques to maximize the quality and quantity of biomass, while the downstream process focused on harvesting and the concrete production of microalgae biomass [16].

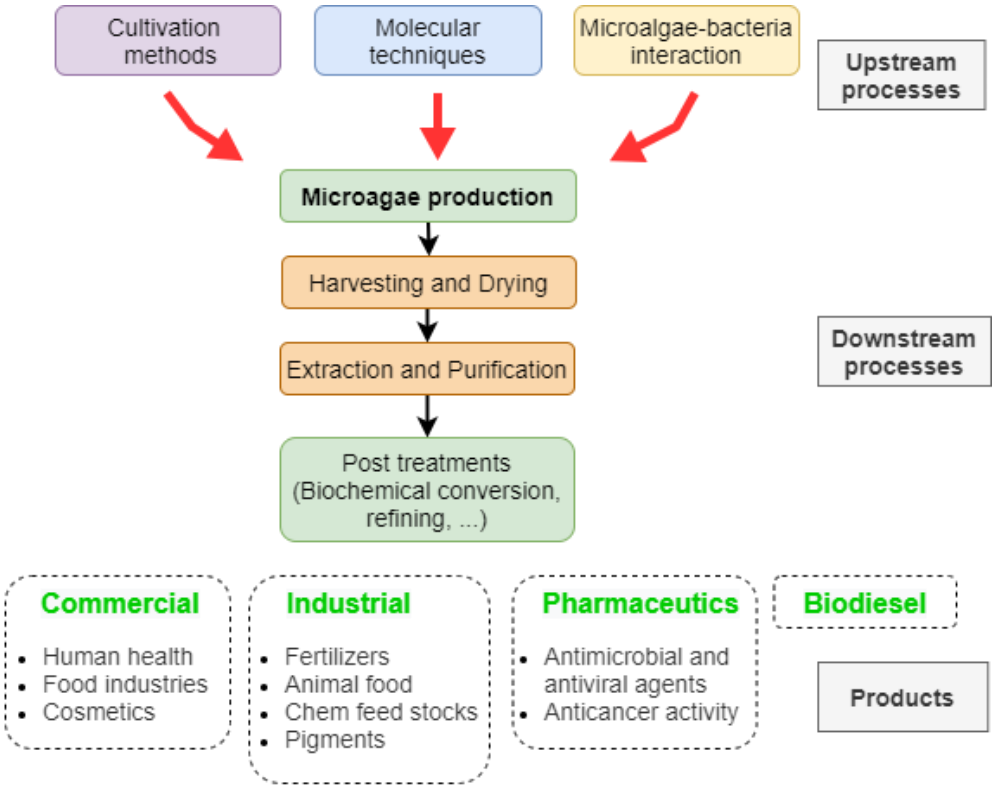

Figure 4 - Production process and products [16].

UPSTREAM PROCESSES

Microalgae production can be done by cultivation in open or closed system, where the growth rate and maximum microalgae production is influenced by abiotic factors (light, temperature, pH, salinity, CO_2, O_2, nutrient), biotic factors (pathogens and competition from other algae) and operational factors (mixing, dilution rate, collection frequency).

There are also other techniques to improve the production of microalgae:

Genetic manipulation in microalgae is relatively easy as single-celled organisms. The main objective is to improve the production of biomass and biodiesel [20]. Progress in the genetic engineering of microalgae has been extremely slow until recently.

Bacterial biofilms to improve biomass production. But only limited studies have been conducted on the existence of interactions between bacterial biofilms and microalgae [16]. These studies suggest that bacteria encourage microalgae growth by producing vitamins and other growth factors, and organic matter produced by microalgae simultaneously encourages bacterial growth.

DOWNSTREAM PROCESSES

Harvesting and dewatering.

After obtaining enough biomass, the microalgae must be separated from the water. According to the life cycle analysis, this separation process accounts for 20-30% of the total production costs of biofuels [20]. Biomass harvesting and drying processes can constitute an important energy consumption in the production of biofuels from microalgae. Therefore, it is necessary to reduce the energy consumption in the harvesting and drying processes of microalgae biomass.

Extraction and purification of lipids.

Different methods such as presses, supercritical carbon dioxide extraction, ultrasound-assisted extraction, osmotic shock, solvent extraction, and enzymatic extraction are available for extracting oil and other precious compounds from microalgae biomass.

When selecting the appropriate extraction process, the most important aspects to consider are cost, efficiency, toxicity, and ease of handling [16].

Microalgae biomass conversion technologies.

The used technologies to convert microalgae biomass are biochemical conversion, thermochemical conversion, chemical reaction, and direct combustion. Biochemical conversion is used to produce methanol by anaerobic digestion or ethanol by fermentation of microalgae biomass. The thermochemical conversion can be classified into pyrolysis to obtain bio-oil and charcoal, gasification, and liquefaction. In chemical conversion technologies, the transesterification process can be used to convert the extracted lipids into biodiesel [10]. Direct combustion is able to directly convert into electricity the energy stored in microalgae cells.

Chapter 2
CULTIVATION SYSTEMS

Depending on the microalgae species, the conditions of the environment, and the availability of nutrients, microalgae can be grown in open systems (open tanks) or closed systems (photobioreactors) [21], here, in Fig. 5, a quick overview is shown.

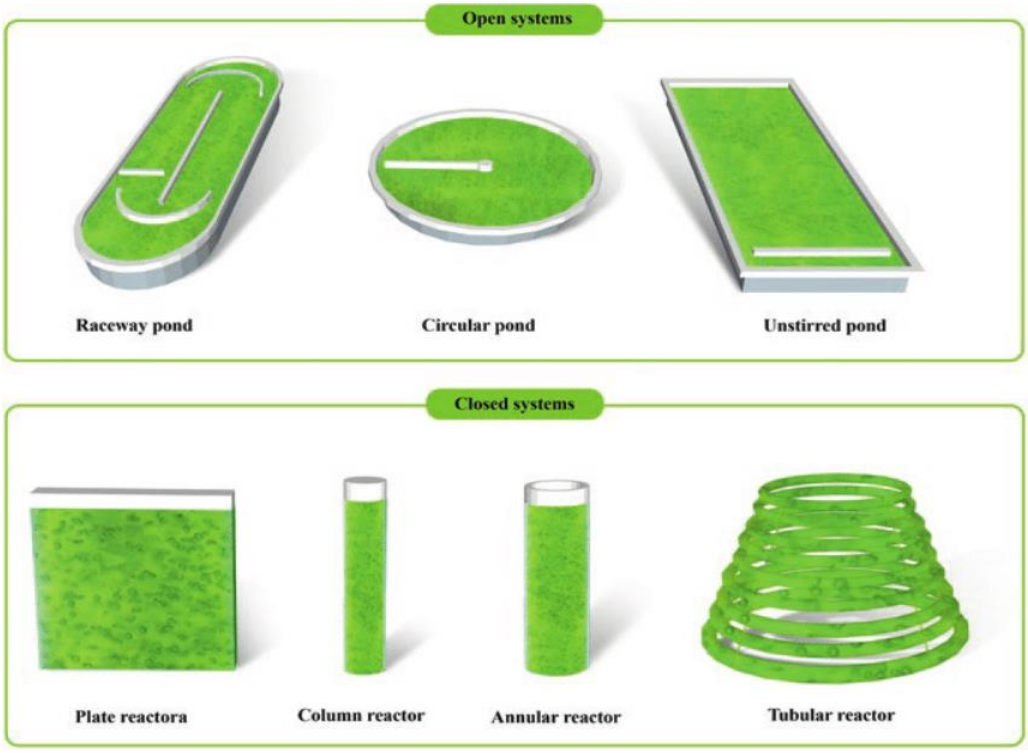

Figure 5 - Common types of microalgae cultivation systems [22].

In both indoor and outdoor microalgae cultivation systems, the light source and intensity are critical factors. Sunlight is the primary light source for outdoor cultivation, while artificial light sources (LED and optical fiber) are used for indoor cultivation systems.

2.1 Open systems

The most widely used open systems are raceway systems, in Fig. 6 they are presented in different scale plant. They are reactors, usually built of concrete and covered with plastic, with a paddle wheel for mixing and circulation. Those raceways have a closed-loop recirculation channel approximately 0.5 m deep to allow the sunlight to penetrate in the culture medium [23].

Figure 6 - Raceways system in different scale farms.

Open systems are less expensive to build, have a longer lifetime, and great production capacity, but they required a large surface. The open systems have a high surface area per volume ratio, allowing high CO2 mitigation [24].

Nevertheless, growing algae outdoors in open pond systems suffered some drawbacks whereby it requires a significant land area, and the culture is subjected to high risk of contamination, and the evaporative water lost can be significant [25].

The outdoor photobioreactors are conditioned by the day-night cycle, while the indoor ones are illuminated by continuous light. In the absence of light, cells can metabolize cellular components for energy, resulting in decreased biomass produced [2]. To solve this problem, prototypes have been developed that allow the switching on and off of an artificial lighting system in order to guarantee continuous lighting even outdoors. Further progress in optimizing light distribution within the crop has been made using optical fibres [26].

2.2 Close systems – Photobioreactors

Photobioreactors (PBRs) can be flat or tubular, horizontal, vertical, inclined, or bags system (Fig. 7). These types of reactors allow you to have better control of the conditions and growth parameters of the crop (pH, temperature, oxygen, CO2), lower losses of carbon dioxide, greater density of microalgae and volumetric productivity, as well as a reduction of contamination by other microorganisms.

Figure 7 - Closed systems, from left: Flat panel PBR, Tubular PBR, and Bags system.

These advantages are even more important if the desired microalgae are used for pharmaceutical purposes or highly selective product applications, in particular for the food market also for cosmetics [20]. The photobioreactors allow working at much higher cell concentrations as they reduce the losses of fresh water, they help the collection of microalgae and reduce the costs related to preparation and handling.

It is important to remember the existence of hybrid systems, which combine the advantages of closed and open systems for the production of microalgae. They use closed PBRs for the inoculum development phase and then, when the algal strain is resistant and dominant, the culture is moved to open reservoirs.

Flat panel photobioreactors are closed systems with the largest surface compared to the volume ratio, and this means having a large irradiated area, a large harvest volume, and excellent biomass productivity [21].

As shown in Fig. 8, this system is mainly composed of rectangular boxes arranged vertically or at an angle where microorganisms can grow. It is often divided into two parts connected to each other to facilitate the process of filling/emptying, gas injection, and transport of nutrients.

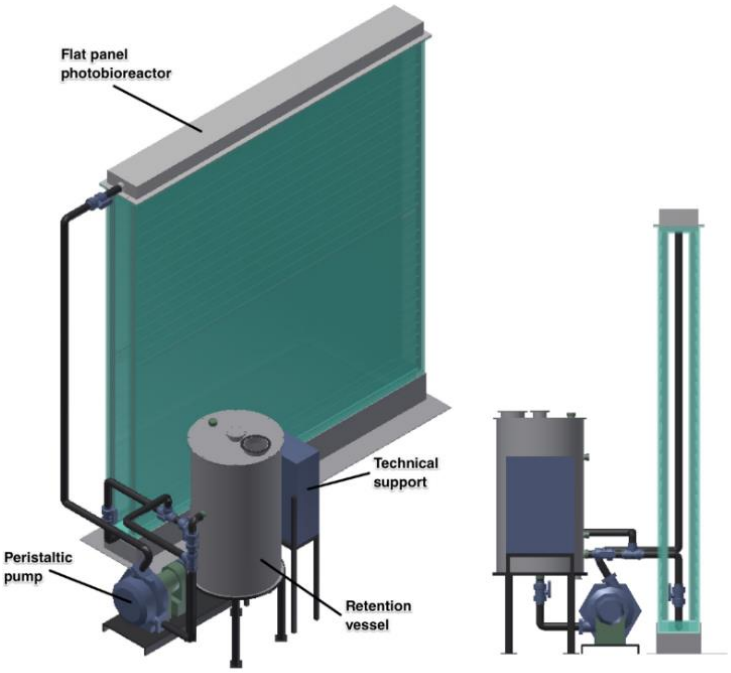

Figure 8 - Common flat plate photobioreactor for microalgae production [27].

The introduction of nutrients occurs mainly at the bottom and in gaseous form to ensure that each compound (mainly CO_2) has sufficient time to interact with the algae in the reactor fluid.

The main drawbacks of flat panel systems are related to the high operating cost due to the aeration and mixing of the solution and to the hydrodynamic conditions inside the chamber that influence the fouling formation, mass, and heat transfer [27].

Ideal PBRs should have a highly transparent surface (avoid fouling formation), minimal non illuminated part, high mass transfer rates in order to obtain high biomass growth [21].

2.3 Main Parameters

The main parameters for proper microalgae cultivation are temperature, light irradiation, pH, salinity of culture medium, utilization of nutrients, and mixing of culture medium.

Temperature

Temperature is a predominant factor in ensuring the protection of microalgae as living organisms. Therefore, having the ability to control this parameter is essential to improve production. Temperature also affects the photosynthetic activity of microalgae. In most cases, an increase in microalgae growth occurs with an increase in temperature until an optimal value is reached. Temperatures below 16 °C and above 35° C are considered fatal for microalgae [28].

Light

Perhaps the most significant parameter to be taken into account during the microalgae growth for fuel purpose, a necessary factor for photosynthesis and therefore for carbon fixation. We have three different light conditions: Light limitation, Light saturation, and Light inhibition.

- If the light is limiting, algae growth decrease with a lack of light intensity.
- Upon light saturation, photosynthetic activity decreases when photon absorption exceeds the amount of electron turnover, thus inhibiting photosynthesis.
- When the light intensity is further increased, irreversible damage to the photosynthetic apparatus occurs. This is called photo-inhibition.

The light intensity and its duration directly affect the photosynthesis process and, therefore, the growth of microalgae. Discovery revealed that microalgae tend to thrive under blue ($\lambda \sim 450$nm) or red ($\lambda \sim 650$nm) light [28].

Additionally, microalgae require periods of light and dark for photosynthesis. It requires light for the photochemical phase and darkness for the biochemical phase. Investigations have shown that the duration of the light intensity increases the growth of microalgae [29].

pH

pH is the parameter that controls cell metabolism and biomass formation in microalgae. The growth of most microalgae species improves a neutral pH and also affects the photosynthesis process in microalgae. For pH values that are too different from neutrality, the rate of photosynthesis is reduced [25].

The pH has a relationship with the concentration of carbon dioxide, i.e. the pH constantly increases as carbon dioxide is consumed. The pH affects the accessibility of nutrients such as iron and organic acids.

Salinity

Each strain of microalgae exhibits differences in adaptation to salinity. Salt stress affects cell growth and lipid formation. It was noted that as salinity increased, lipid expression increased but resulted in cell growth. Marine microalgae are obviously more tolerant to alterations in salinity than freshwater species [25].

Nutrients

Carbon and hydrogen are nutrients necessary for growth, and they are generally available in enough quantities. Mineral nutrients include nitrogen, phosphorus, potassium, magnesium, and sulphur. Traces (<4 ppm) of iron, manganese, cobalt, zinc, boron, copper, and molybdenum are also needed [31].

The nutrients needed for microalgae can be provided by industrial, agricultural, municipal, and food wastewater. However, wastewater can also contain toxic chemicals that can harm microalgae, so they need to be analysed carefully.

For carbon, we can use CO_2 from the atmosphere, or from industrial exhaust gases. Using flue gasses as a carbon source makes the entire cultivation process cheaper, contributing to the development of viable and sustainable cultivation techniques for producing microalgae biomass.

Carbon dioxide

Today, global energy demand is almost entirely met by fossil fuels, generating an enormous amount of CO2. One solution could be the biological fixation of carbon dioxide [30].

Microalgae can fix carbon dioxide more efficiently than terrestrial plants. The quantity of carbon dioxide available for the culture plays an important role in the growth of microalgae. If the concentration of carbon dioxide is high enough, the microalgae grow more.

Mixing

Mixing is necessary to guarantee the uniform distribution of nutrients, air, CO2, temperature and, light in microalgae culture. It also prevents the biomass from settling and causing aggregation. In fact, microalgae cultures must be continuously mixed to keep all cells in suspension with free access to light.

If all the other factors are met, but there is no mixing, biomass productivity will be lowered significantly [25].

Chapter 3
MIXING

The mixing does not directly affect the growth of microalgae. However, it is essential to ensure optimal levels within the entire culture of all the parameters indicated in the chapter above, such as nutrients, temperature, and even light [28].

The illumination and temperature of microalgae crops depend on each other. The strict control of both is difficult and costly. Mixing is the most practical way to ensure uniform light distribution to all cells.

The mixing systems depend on the geometry and the type of reactor. For the classic raceway reactors, the mixing system most used today is a cylindrical rotor (Fig. 9), with a horizontal axis, equipped with paddlewheels [32]. The movement of the blades guarantees the exchange of substances with the atmosphere and the mixing of the crop, reducing the problem of sedimentation.

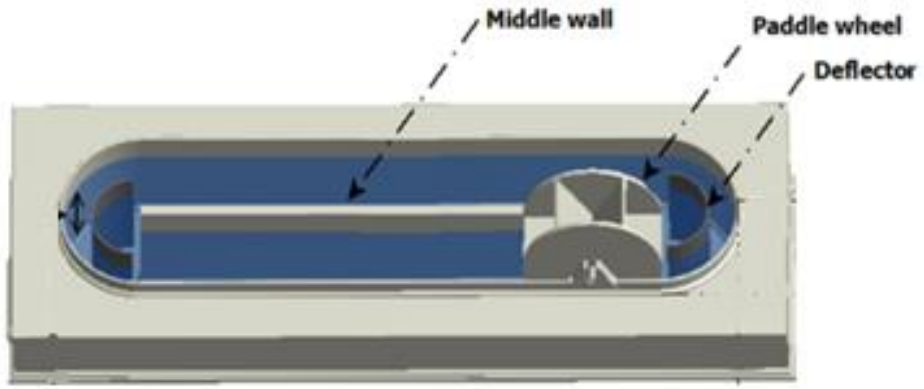

Figure 9 - Raceway system equipped with paddlewheel.

However, due to the contamination of the crops and the evaporation problem in the open system, the productivity of the plant is limited, but the operating costs of the open photobioreactors are very low since the lower density of the solution, and this minimizes the energy required to keep the fluid agitated [32].

In closed photobioreactors, crop agitation systems are certainly more expensive and sophisticated. Inside a closed PBR, it is very hard to have adequate handling of CO_2 due to the absence of contact between microalgae biomass and the atmosphere. Therefore, there is a tendency to insufflate carbon dioxide to enrich the solution by bubbling the gas directly into the liquid and consequently mixing the entire crop through the air diffusion.

The mixing of the microalgae biomass in a closed bioreactor can also be carried out with mechanical pumps for recirculation of the entire culture and by mechanical or pneumatic agitators, but the latter technology is not always applicable in a flat panel reactor, and also it offers important disadvantages such as high shear forces which can damage microalgae cells, and then stirred tank PBR are not easily scalable [33], [34]. Therefore, applying the static mixer seems to be the best option.

The problem examined in this thesis represents a particular situation of an innovative context; for this reason, different types of static mixers, widely used in various industrial fields, have been analysed to highlight the mixing principles through a passive obstacles/barrier.

A study of the mixers available on the market and an evaluation of the technical characteristics and their possible use in flat PBR panels were carried out. The most interesting are here represented.

3.1 Static mixer

Static mixers are mainly used to mix fluids with different viscosities and densities. Generally, in the hydraulic pipeline in which the static mixer is inserted, external pumps are used to create the fluid flow inside the mixer. The fluid moment is converted into static mixing mechanical energy at the expense of the pressure drop [35]. In fact, since the static mixers have no moving elements, the mixing depends

exclusively on the movement of the flows, which, according to the internal geometry of the mixer, are rotated, twisted, split, and recombined.

The main consequence of the static mixer is the pressure drop that is precisely the energy supplied by the external pumps. From an engineering point of view, an ideal static mixer leads to the desired mixing with minimal pressure drop [36].

The mixer is dependent on the type of solutions to be mixed. In fact, mixing is strongly influenced by the shape and size of the particles, by the density and viscosity of the solution. The quality of mixing can be improved by changing the shape, size, and number of elements inside the mixing tube.

3.1.1 Helical static mixers

This type of static mixer has a helical mixing element inserted inside a tube, as shown in Fig. 10. This mixing element provides a flow splitting for any combination of liquids, gases, or solids and full radial mixing [35].

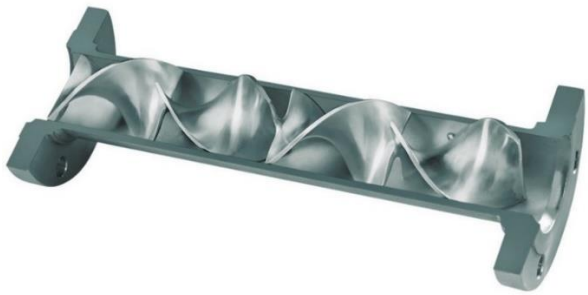

Figure 10 - Helical static mixer element in a tube.

Homogenization of the solution is mainly based on (Fig. 11), [35]:

1. Flow Division: As the product stream passes over each mixer element, it is divided into two halves. If n is the number of mixing elements, the divisions of the fluid grow exponentially equal to 2n.

2. Radial Mixing: The flow is forced to be entirely inverted so that particles entering at the center of the stream are continuously moved to the outer wall and back again.

3. Rotational Circulation: The first helical element rotates the flow in one direction, then the direction is reversed at the next element.

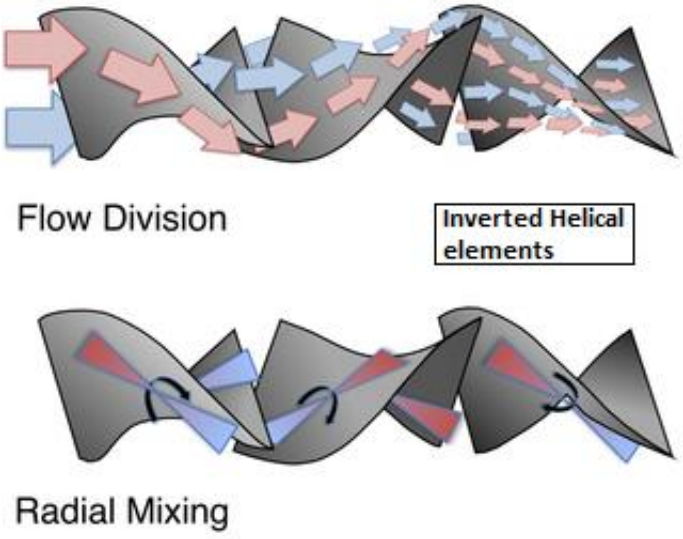

Figure 11 - Mixing principles in a helical static element.

Static mixers with the helical structure are cheap and with moderate mixing capacity over wide flow ranges, particularly suitable for laminar flow and high viscosity applications where the mixing task is simple, but they are also characterized by low-pressure drop [37].

3.1.2 Wavy sheets static mixer

This type of static mixer aims to intensify the mass transfer between immiscible fluids, the wavy plates form open and intersecting channels (Fig. 12), in which the flow is divided into many secondary flows.

This static mixer is used in turbulent and transition flow regimes and offers a high performance by mixing liquids, low viscosity gases or to disperse immiscible liquids and create gas-liquid dispersions with a very high degree of mixing in a short time while keeping the fabrication cost low [38].

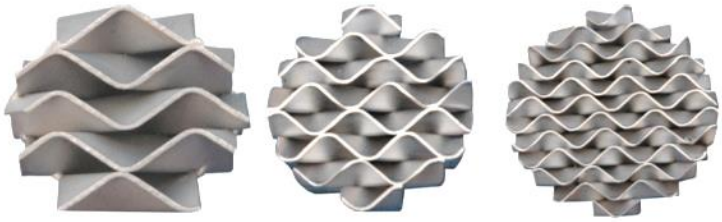

Figure 12 - Wavy sheets.

3.1.3 Multilayer static mixer

The multi-layer static mixer, shown in Fig. 13, repeatedly divide the fluid flow into several layers and distribute them over the entire cross-section of the pipe. A big advantage of this type of design is that it can mix extremely high viscosity fluids.

Figure 13 - Multilayer elements.

The mixing is done in a short time with a very high degree of mixing. Reducing residence times can be helpful in cases where product degradation is a problem. And also, the possibility of performing an optimal mixing service with a smaller mixer, consequently also reducing the pressure drop [38].

3.1.4 Open static blade mixers

Also, in this case, mixing is obtained by splitting and deflecting the incoming fluid flows, but there is an open channel without the presence of blades (Fig. 14). The main advantage of this design is that, in turbulent flow applications, it improves the random dispersion of secondary flows.

For example, Chemineer has patented HEV Mixer (Fig. 14), a static mixer with a high efficiency open blade design. The HEV offers lower pressure losses, and it can

handle any turbulent flow mixing process regardless of size or shape. Mixing is performed by controlled vortex structures generated by a patented tongue geometry, which provides uniform mixing by limiting the length to less than 1-1/2 tube diameters [39].

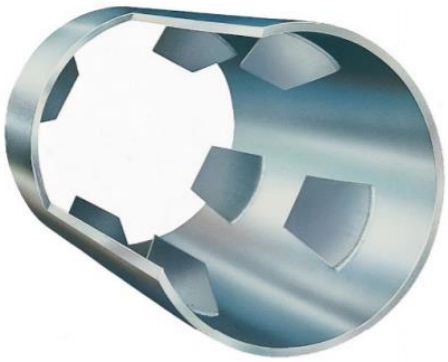

Figure 14 - HEV Mixer, open blade static mixer from Chemineer [39].

Static HEV mixer is typically used for low viscosity liquid-liquid mixing processes and gas-gas mixing processes. HEV can be found for non-circular cross-sections, effective mixing of additives in places not suitable for traditional static mixers. It is particularly suitable for gas phase processes where pressure loss and length are critical [39].

Chapter 4
OBJECTIVES AND THESIS OUTLINE

In order to improve the production of microalgae and to make it technically and commercially viable, it is necessary to improve every single step of the production process (Subchapter 1.4 Production process) and take into account all the parameters related to microalgae growth.

It has been chosen to focus on the growth phase of microalgae, using a flat panel PBR: the best reactor where you can control all parameters, such as light and nutrients, it supports a higher growth rate and higher photosynthetic efficiency, and it is possible to obtain high quality of microalgae biomass [10]. However, there are some drawbacks, such as the high costs of construction, operation, and maintenance. The aeration and agitation costs can represent about 80% of the production costs of microalgae, and they can reduce the whole yield of the process [2], [40].

Therefore, the tendency is to develop PBR with effective and inexpensive agitation and aeration systems to increase biomass productivity. An efficient mixing system improves mass transfer, eliminates light gradients, and ensures homogeneous mixing of nutrients.

In this case study, the microalgae culture has been continuously recirculated through a pump, but it has been decided to introduce an inclined perforated plate (IPP) system, an innovative static mixer capable of mixing all the fluid within the entire volume of the chamber.

The aim is to work on the hydrodynamic conditions inside the flat panel by introducing a static mixer system to improving the growth and production of microalgae biomass by minimizing pressure drops, trying to understand if the presence of a static mixer can actually make the process economically feasible or it is necessary to act on other parameters.

This thesis aims to develop a stable mathematical model that can be used to evaluate the efficiency of the given mixer geometry.

This mathematical model is a quantitative representation of a natural phenomenon, and its purpose is to represent it, in as much detail as possible. Starting, therefore, from real-world data, a mathematical model was formulated with the Ansys software that reflects it as much as possible [41].

4.1 Strategy of work

This work was divided into three levels: design phase, CFD Analysis of IPP system, and experimental validation. According to the following scheme shown in Fig. 15:

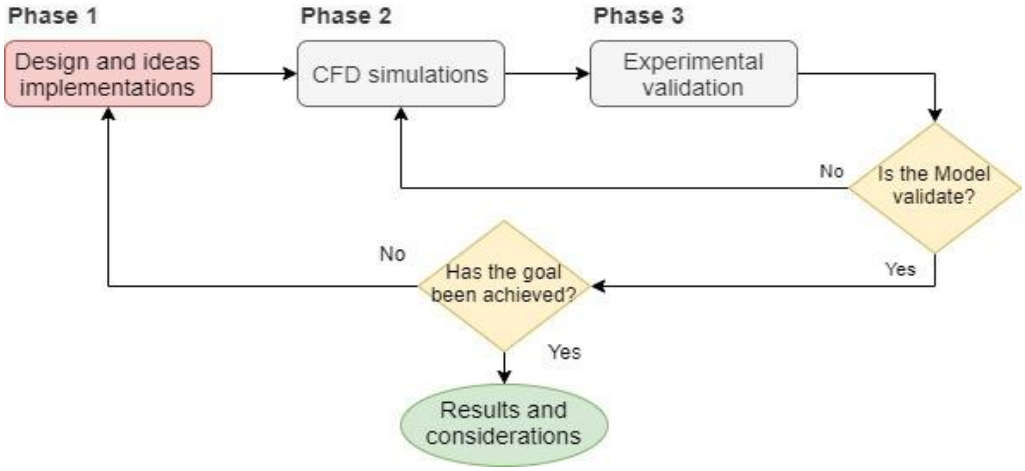

Figure 15 - Strategy of work.

The first phase was the most creative part where the aim was to test several "elementary" geometry through CFD simulations just to better understand the complex situation, and which parameters were more important during the mixing in a flat panel, so it was possible to define an optimized geometry of the static mixer system, before building the prototypes, saving time and money.

For the first design phase, only the configurations that are most useful for the comprehension of the work are shown here. They are: Empty flat panel, Horizontal plates in flat panel, and a 5-degree IPP system into a flat panel.

Once the final geometry was chosen, more accurate simulations and data were collected. The direct comparison between the Empty flat panel configuration and

the one with the IPP system installed has been useful to deepening the hydrodynamic studies.

Then the experimental validations phase, where the configurations decided, has been realized and then will be tested in the laboratory. These validations will take place through hydrodynamic parameters that can be easily measured in the laboratory, such as the pressure drop, but the experimental part, or 3rd phase was not included in this thesis. The experimental validation of a developed numerical model should be the aim of further work.

Chapter 5
CASE STUDY

The used technology was a flat panel photobioreactor with two chambers (Fig. 16), and it was possible to use them separately. The dimension of each chamber is 1020x750x65 mm, as is shown in Table 2. The working volume of one PBR chamber is about 50 l. The experiments were focused only on one chamber.

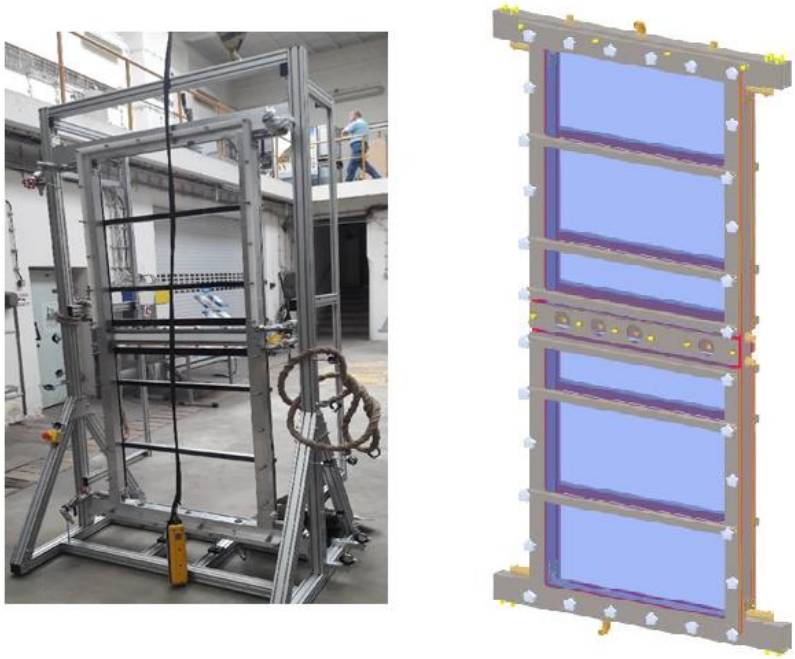

Figure 16 - Flat panel photobioreactor examinate.

The movement of the fluid and the energy needed to maintain the correct recirculation are provided by a peristaltic pump that will operate continuously in the closed-loop of our system. A peristaltic pump is installed, and it was able to guarantee a variable flow rate from 0 - 100 litres per minute.

Peristaltic pump

The peristaltic pump is a device that applies the principle of peristalsis, or the prevalence of the treated fluid is given by an astriction that runs along the tube. The peristaltic pump consists of a rotor with two or more rollers which, by rotating, "throttle" the tube and make the fluid advance (Fig. 17).

The main component of the pump is the tube which is usually made of materials such as silicone, PVC, and other polymers which offer adequate mechanical characteristics and chemical compatibility [42].

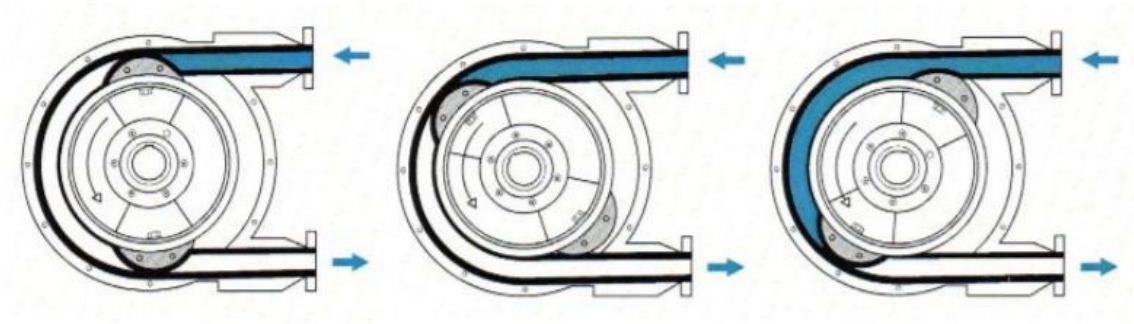

Figure 17 - Working principles of peristaltic pump.

The peristaltic pump is a "pulsating" pump, as the flow rate is not constant over a single revolution. A greater number of rollers can be used to reduce the pulsation phenomenon, with a consequent reduction in the flow rate, or compensators can be used which absorb the "pulsation peak" until a constant flow rate is obtained.

The peristaltic pumps are used when the treated fluid must not come into contact with the pump components:

- To avoid contamination, such as in the food, pharmaceutical, and medical fields (extracorporeal circulation, dialysis).
- If the fluid is aggressive, acidic, or harmful to the pumping organs (solvents, fuels, chemical reagents, etc.).
- When fluid with suspended and fragile solid bodies must be transferred without being damaged.

The process flow diagram of the flat panel PBR is shown in Fig. 18. The transparent PBR chamber, the retention vessel, and the peristaltic pump were the main components. Nutrients were added to the culture medium, and the produced oxygen is desorbed in the retention vessel. The peristaltic pump ensured the flow of the culture medium and its homogenization.

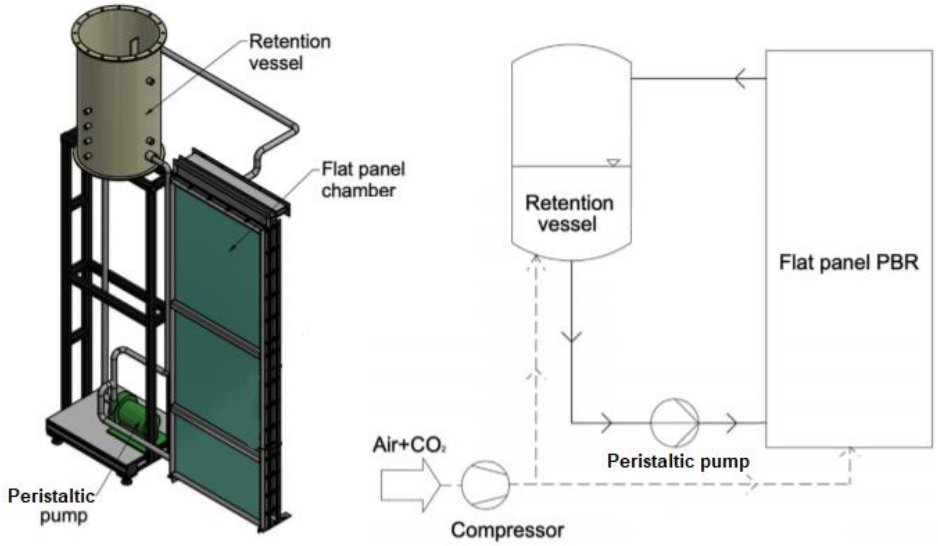

Figure 18 - Process flow diagram of flat panel PBR set up.

Geometry of PBR chamber

Dimension	Value	Unit
Heigh H	1,02	m
Length L	0,75	m
Thickness S	0,065	m
Volume V	49,7	litres

Table 2 - Geometry parameters.

5.1 Inclined Perforated Plates system

This system was designed with the idea that one of the most important parameters to optimize microalgae growth is light. In the production reality, this translates into maximum transmission capacity and transmission efficiency, understood both as losses and the fluid's ability to absorb this light [7].

Mixing helps to absorb the same amount of light to each organism, but an excellent mixing system shouldn't block incoming light. Therefore, a static mixer system was designed with a minimum surface in the normal direction of light impact, as shown in Fig. 19.

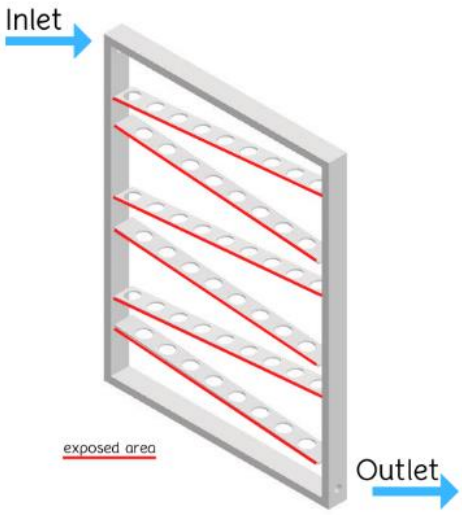

Figure 19 - 3D model of IPP system.

This has been translated into a static mixer formed by thin perforated plates, integrated directly with the internal surface of the front wall of the flat panel photobioreactor.

Two types of perforated plates were glued, alternately, directly on the front panel of the flat panel. These 2 types of plates have the same dimensions (730x65x5 mm), but they have the holes arranged staggered to create an obligatory path for the microalgae culture, to have a better distribution inside the chamber.

Plate type A has 9 holes of diameter 45 mm, while **plate type B** has 8 holes of 45 mm. In both plates, the center distance is 83 mm (Fig. 20). The absence of one hole on the plates type B creates a different passage area; therefore, pressure and velocity at alternating sections also guarantee better mixing.

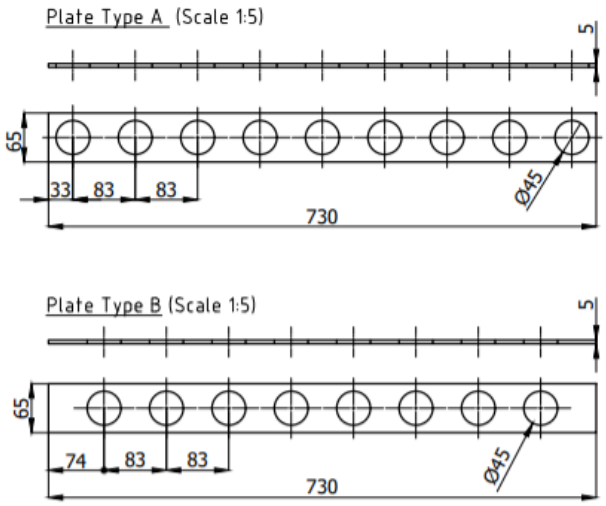

Figure 20 - Hole arrangement: plate type A (top), plate type B (Bottom).

Furthermore, after some CFD simulations, it was decided to incline the plates to intercept the inlet flow in the best possible way and to avoid sedimentation phenomenon significantly (thanks also to the minimum roughness of the chosen material); for the latter reason, the plates are shorter than the internal length of the chamber, this to facilitate the "drainage" of the microalgae culture. Furthermore, this choice constitutes an excellent constructive solution because by tilting the plates, the sheet should have been cut with an appropriate contact angle to allow the connection, it would translate into additional production costs.

The thickness of the plates is 5 mm to ensure the minimum bonding surface and, above all, to avoid bending during use.

A further constructive aspect taken into consideration is the size of the passage holes. Having a large diameter allow a less aggressive mixing that allow minimizing damage to the microalgae.

In Table 3 are summarized the advantages of the static mixing system designed.

Advantages of IPP System	
SMALL AREA IN THE NORMAL DIRECTION	Maximum light transmission
INCLINED PLATES	No sedimentation
DESIGN	Not-aggressive mixing
SIMPLE GEOMETRY	Low costs

Table 3 - IPP system advantages.

The chosen configuration has the IPP system installed with 5 degrees of slope, but this was the result of a long process of selection through CFD simulations: started with an empty chamber, then a primordial IPP system with not inclined plates, and at the end, different slopes were applied at the plates.

Chapter 6
COMPUTATIONAL FLUID DYNAMICS

Fluid dynamics is the branch of dynamics that studies fluid flows and their forces, while Computational Fluid Dynamics (CFD) is the methodology for predicting such fluid flows, heat and mass transfer, and related phenomena by solving equations for the conservation of mass, momentum, energy. CFD can provide detailed information on fluid flow behaviour such as distribution of pressure, velocity, temperature, or forces such as lift and drag [41].

A typical CFD solver is based on the finite volume method. This means that the domain of the model is discretized into a finite set of control volumes, and the general conservation (transport) equations for mass, momentum, and energy are solved on these volumes. Then the partial differential equations are discretized into a system of algebraic equations, and finally, all the algebraic equations are then solved numerically [43].

In this work, CFD has been used to conceptualise new geometries and their optimization, reducing the total effort and the cost of the eventual prototyping phase.

6.1 Main equations

There are 2 main equations in CFD required in this thesis, and they are based on the principles of conservation of mass (the continuity equation), momentum (Navier Stokes equation) [41].

Continuity equation of mass

The continuity equation of mass describes the mass balance of a system in a determined control volume. For incompressible fluids, where the density of the fluids is constant, it is described as:

$$\nabla \cdot \vec{u} = 0 \tag{2}$$

Where the vector $\vec{u}$ is the velocity. The eq. 2 can be extended in Cartesian coordinate as:

$$\frac{\partial \bar{u}}{\partial x} + \frac{\partial \bar{v}}{\partial y} + \frac{\partial \bar{w}}{\partial z} = 0 \tag{3}$$

Where $\bar{u}, \bar{v}, \bar{w}$ represent the velocity components in the 3D directions x, y, z and $\partial x, \partial y, \partial z$ are the lengths of the fluid element analysed in the same 3D space.

Navier-Stokes equation

The Navier-Stokes equation represents the equilibrium of momentum and is a special case of the Cauchy equation. It is applied for non-compressible Newtonian fluids (constant density) and gravity forces rather than volume forces [41]. This equation can be written as:

$$\rho\left(\frac{\partial \vec{u}}{\partial t} + \vec{u} \cdot \nabla \vec{u}\right) = \rho \vec{g} - \nabla p + \mu \nabla^2 \vec{u} \tag{4}$$

Where the vector $\vec{u}$ [m/s] is the velocity, ∇p [Pa] is the pressure gradient, μ is the dynamic viscosity, ρ [kg/m^3] is the density and g [m/s^2] is the force of gravity.

6.2 Turbulent modelling

Turbulence is a state of fluid characterized by the generation of some structures as eddies and vortex (zone with a rotating volume of fluid); usually, in turbulent flow, it is possible to find many scales of eddies. Turbulence is essentially a random process characterized by fluctuations of transported quantities such as flow velocity, pressure, temperature [43].

The actual velocity of a real (turbulent) flow is represented in Fig. 21:

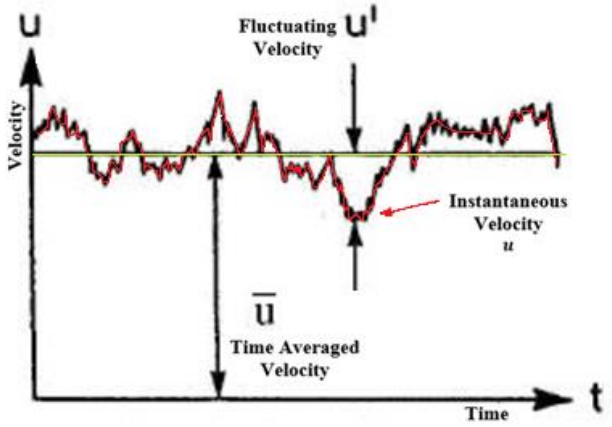

Figure 21 - Actual velocity in real flow [44].

It can be described as:

$$\vec{u} = \bar{u} + u' \tag{6}$$

Where $\bar{u}$ is the mean velocity and u' [m/s] is the fluctuating velocity.

Turbulence modelling is a complex area because of the random behaviour of the flow, therefore it is not possible to perfectly describe the turbulence effects in a CFD simulation; however, there are several ways to model a turbulent regime with so called turbulence models, such as direct numerical simulation (DNS), large eddy simulation (LES) or Reynolds averaged Navier Stokes (RANS) [41], [45].

In this work, Reynolds averaged Navier Stokes (RANS) model in 2 equation model (k-Ɛ model RNG) is used, and it is only discussed here.

By substituting the actual velocity in terms of average and fluctuating velocity components (eq. 6) into the Navier–Stokes equation (eq. 4), it is possible to obtain the RANS equation for mean velocity:

$$\rho\left(\frac{\partial \bar{u}_i}{\partial t} + \bar{u}_k \frac{\partial \bar{u}_i}{\partial x_k}\right) = -\frac{\partial \bar{p}}{\partial x_i} + \frac{\partial}{\partial x_j}\left(\mu \frac{\partial \bar{u}_i}{\partial x_j}\right) + \frac{\partial R_{ij}}{\partial x_j} \tag{7}$$

Where R_{ij} is the Reynolds stress tensor, which must be described by a turbulence model.

Following the Boussinesq hypothesis, where it is assumed that, as in laminar flows, the viscosity is analogous to the shear stresses, the turbulent viscosity should be analogous to the mean velocity gradient [46]. For incompressible flows, under the Boussinesq hypothesis, it is possible to define Reynolds stress tensor as follows:

$$R_{ij} = -\rho\overline{u_i' u_j'} = \mu_t\left(\frac{\partial \bar{u}_i}{\partial x_j} + \frac{\partial \bar{u}_j}{\partial x_i}\right) - \frac{2}{3}\mu_t \frac{\partial \bar{u}_k}{\partial x_k}\delta_{ij} - \frac{2}{3}\rho k \delta_{ij} \tag{8}$$

Where μ_t, the so-called turbulent viscosity is defined as:

$$\mu_t = \rho C_\mu \frac{k^2}{\varepsilon} \tag{9}$$

where C_μ is an empirical constant, k is the turbulent kinetic energy, and ε is the dissipation rate of the kinetic energy.

6.3 Model

In the present work k-ε turbulent model (2 eqn), "RNG" is used.

The k-ε model is simple but robust. The two-equation turbulence model of the k-ε type was derived by using Renormalization Group (RNG) methods. In the standard k-ε model, the turbulent kinetic energy is solved for two variables, k, and the rate of dissipation of kinetic energy, ε [45], [47]. But using the modification as renormalization group (RNG) k-ε model, the simulation produces lower turbulence levels and can underestimate the value of k. This produces a less viscous flow that creates more realistic flow features with complex geometry.

The effective viscosity is calculated through equation 9, and it requires the values of k and ε, which are determined from the following transport equations [45], [48].

The transport equation for k is:

$$\frac{\partial \rho k}{\partial t} + \frac{\partial}{\partial x_i}(\rho \upsilon_i k) = \frac{\partial}{\partial x_i}\left[\frac{\mu_t}{\sigma_k}\frac{\partial k}{\partial x_i}\right] + G_k + G_b - \rho\varepsilon - Y_M - S_k \tag{10}$$

and the transport equation for ε is:

$$\frac{\partial \rho \varepsilon}{\partial t} + \frac{\partial}{\partial x_i}(\rho v_i \varepsilon) = \frac{\partial}{\partial x_i}\left[\frac{\mu_t}{\sigma_\varepsilon}\frac{\partial \varepsilon}{\partial x_i}\right] + C_{1\varepsilon}\frac{\varepsilon}{k}(G_k + G_{3\varepsilon}G_b) - C_{2\varepsilon}\rho\frac{\varepsilon}{k}\varepsilon + S_\varepsilon - R_\varepsilon \qquad (11)$$

Where μ_t is the turbulent viscosity, Y_m represents the contribution of the fluctuating dilatation in compressible turbulence to the overall dissipation rate, G_k is the generation of turbulence kinetic energy due to the mean velocity gradients, G_b is the generation of turbulence kinetic energy due to buoyancy, $C1\varepsilon$, $C2\varepsilon$ are empirical constants, σ_k, and σ_k are the turbulent Prandtl numbers, S_k and S_ε are source terms defined from the user.

The main difference between the RNG and standard k-ε models lies in the additional term in the transport equation for ε, R_ε.

$$R_\varepsilon = \frac{C_\mu \eta^3 (1 - \eta/\eta_0)}{1 + \beta\, \eta^3}\frac{\epsilon^2}{k} \qquad (12)$$

Where $\eta_o = 4{,}38$, $\eta \equiv S_k/\varepsilon$, and $\beta = 0{,}012$. The derived values of $C1\varepsilon$=1,42, $C2\varepsilon$=1,68, $C\mu = 0{,}0845$, $\sigma_k = 1{,}0$ and $\sigma\varepsilon = 1{,}3$. are used in RNG model [45].

Thanks, this term, the RNG model is more responsive to the effects of rapid strain and streamline curvature than the standard model.

RNG based model should give substantially better predictions than the standard k-ε model for turbulent flow over a backwards-facing step [49]. The improvements obtained from the RNG k-ε model were attributed to the better treatment of near-wall turbulence effects.

Chapter 7
SIMULATION PHASE

7.1 Target data

The study of mixing and, therefore, of the fluid behaviour is a complex hydrodynamic problem due to the obvious turbulence to be obtained. It is essential to study, through CFD simulations, the motion of the fluid inside the flat panel to understand how it interacts with the elements that have been installed in the chamber and the chamber itself. The purpose is to obtain a fluid in a continuous movement without stagnant areas, that is, the complete circulation of all the fluid coming from the inlet nozzle through most of all regions of the chamber.

The following parameters and simulations were analysed to understand how the flow moves inside the flat panel chamber:

Volume Rendering: Using a volume rendering option in CFD software gives the flow an effect as if the flow has a dye in it to visualize it. It shows the flow pattern occurring in the flow.

Streamlines are used to conduct a particle path visualization. It is possible to specify the beginning point, and from that point, it follows up the particle's path. With the streamlines, it is possible to see where the regions of circulation are occurring in a 3D domain.

Vector plots are used to identify the flow direction.

Vortex core region to visualize regions of high energy concentration in 3D regions. The vorticity and swirl strength were analysed. The first one is a pseudovector field that defines the local spinning motion of a continuum near some point, it describes the tendency of something to rotate, as it would be seen by an observer located at that point and travelling along the stream, and the second one,

the Swirling strength is an effective vortex indicator in wall turbulence, and it can be determined based on three-dimensional(3D) velocity fields. The swirling strength of the vortex core region represents the strength and the density of the local swirling motion.

The nominal residence time or **hydraulic retention time** (HRT) of a reactor, calculated on a geometric basis, is the ratio between the reactor volume V [m^3] and the total volumetric flow rate of the fluid $\dot{V}$ [m^3/s].

$$HRT = \frac{V}{\dot{V}} \tag{13}$$

Residence time

In the presence of non-ideal mixing due to phenomena such as channelling (one or more parts of the system have different velocity), fluid stagnation (reactor areas with very low speeds), internal recirculation and losses (Fig. 22), residence time follows a probability of distribution [50].

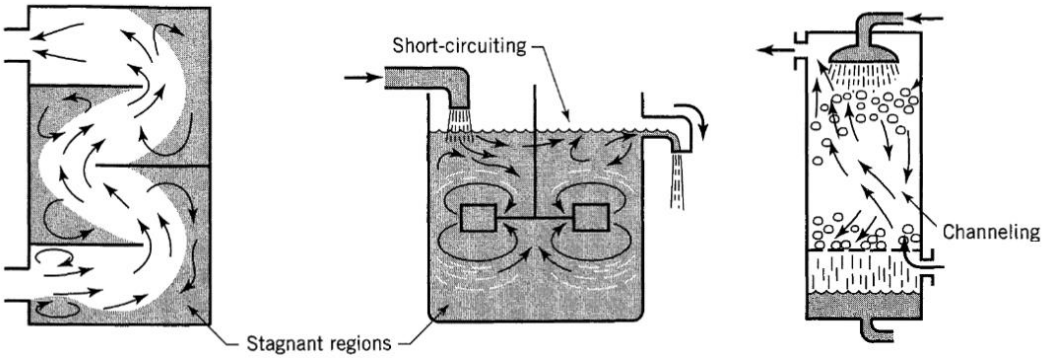

Figure 22 - Non-ideal flow patterns that exist in process equipment [51].

In fact, it is evident that elements of fluid taking different paths through the reactor may take different periods to pass through the vessel. The distribution of these times for the fluid flow leaving the vessel is called the E (time^{-1}) exit age distribution, or fluid residence time distribution RTD. It is useful to represent the RTD in such a way that the area under the curve is unity (Fig. 23), or the fraction of material that has resided in the reactor from 0 to ∞:

$$\int_0^\infty E \; dt = 1 \tag{14}$$

The *E* curve is the distribution needed to account for nonideal flow.

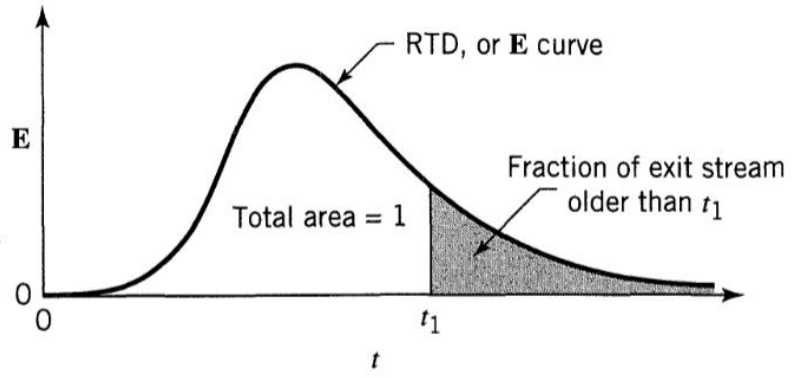

Figure 23 - The E curve, or RTD, for fluid flowing through a vessel [51].

The RTD of the flowing fluid can be determined directly using a non-reactive tracer injection. [51].

Consider $\dot{V}$ [m³/s] of fluid flowing through a reactor with volume V [m³]. At the time **t = 0,** a tracer injection with concentration C_{max} [kg/m³] is performed, and the concentration of tracer output C_{step} is measured in time, t (Fig. 24).

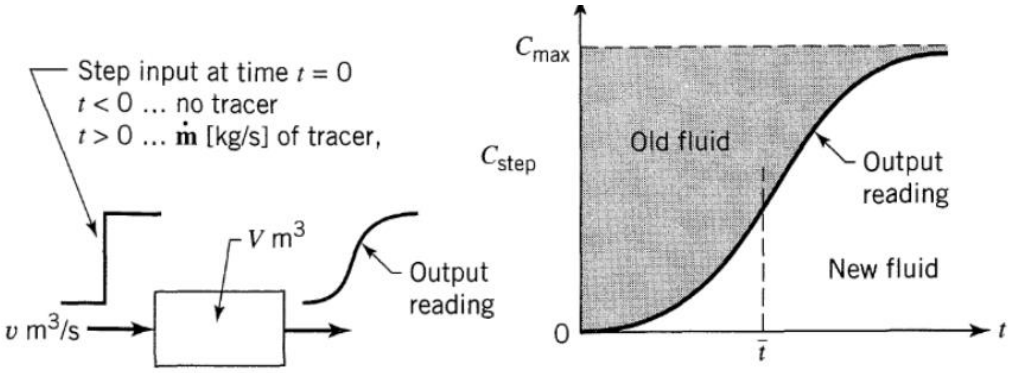

Figure 24 - Tracer step injection [51].

In a step injection experiment, the concentration of the tracer at the reactor input goes directly from 0 to C_{max}. The tracer concentration at the output is normalized to obtain the non-dimensional curve F (t):

$$F\ (t) = \frac{C(t)}{C_{max}} \tag{15}$$

The dimensionless form of the C_{step} curve is called the F curve, or cumulative RTD, and it is found by increasing the concentration of the tracer from zero to unity [51].

Thank the RTD is possible to predict conversion and mixing also in non-ideal reactors.

The **total homogenization time** is a measure of the ability of a given reactor to distribute the fluid within the entire volume of a reactor. The shorter the homogenization time, the better the system. To measure the homogenization time, the most problematic death zone in a reactor must be identified. Then, thanks to a tracer injection, it is necessary to measure, by a control point, when the tracer completely reaches the specified death zone, thus indicate that a full homogenization has been obtained.

7.2 Method

A stable mathematical model has been defined to evaluate the efficiency of the given mixer systems. ANSYS Fluent 2020 R2 software is used as a computational tool.

7.2.1 Mesh

Creating a quality mesh means dividing a continuous geometric space into the right number of discrete elements of adequate size. To determine the quality of the mesh, it has been used 2 fundamental parameters: Skewness and Orthogonal quality [41].

The skewness is defined as the difference between the shape of the cell and the shape of an equilateral cell of equivalent volume, while mesh orthogonality refers to how close the angles between the faces of adjacent elements are to an optimal angle. A general rule is that the maximum skewness for a triangular/tetrahedral mesh in most flows should be kept below 0,94, and the minimum value of mesh orthogonality has to be higher than 0,1.

In this case, for the configuration with the IPP system installed, it was tried to generate the mesh with the proximity capture command on, because the small gap between each plate and the wall could have ruined the entire meshing process.

The proximity capture command allows having a better quality of elements (small size, higher number) in the narrow gap (Fig. 25).

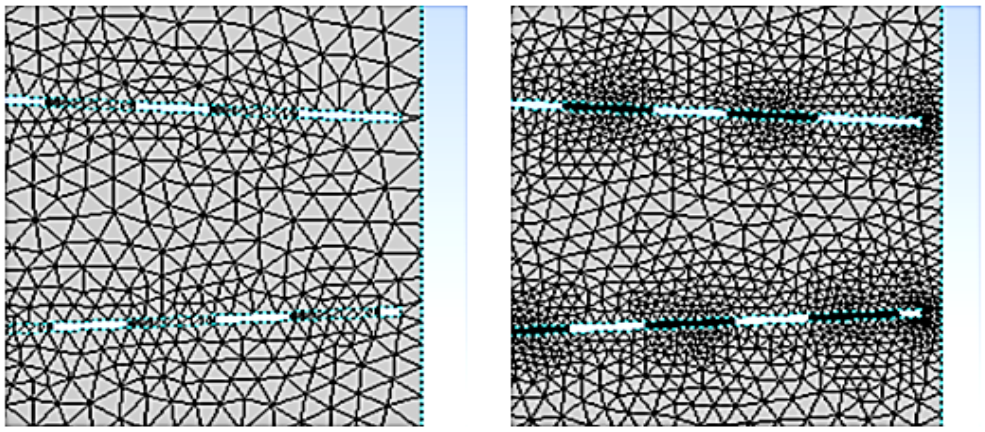

Figure 25 - Meshing comparison.

As reported in Table 4 below, it is possible to see how much this command can improve meshing quality in these specific cases. The main problem with this setup is that the number of elements increases a lot and exceeds the limits of the student version of Ansys.

Mesh Quality

Config	Type	Skewness (Max < 0,94)	Orthogonal quality (Min > 0,1)
Empty	Standard	0,79854	0,20141
	Prossimity capture + standard	-	-
Horizontal plates	Standard	0,895	0,105
	Prossimity capture + standard	0,8445	0,15542
IPP system (5°)	Standard	0,87115	0,12885
	Prossimity capture + standard	0,8425	0,1575

Table 4 - Quality of mesh.

However, the quality achieved with the standard mesh process is enough for simulations, and it has been selected the smallest size for elements respecting the limit in number of elements of the student version of Ansys. This is because it is required to model a vortex situation well, and CFD cannot study vortices smaller than the element size.

Inflation layer

For the 2nd study phase, aimed at deepening the IPP system, the inflation layer was added on the chamber perimeter and on each perforated plate (Fig. 26 B) to better model the turbulent behaviour. Both inflation layers have 5 layers with a growth rate of 1; these values have been chosen to ensure the achievement of the skewness and orthogonal quality values indicated in Table 5.

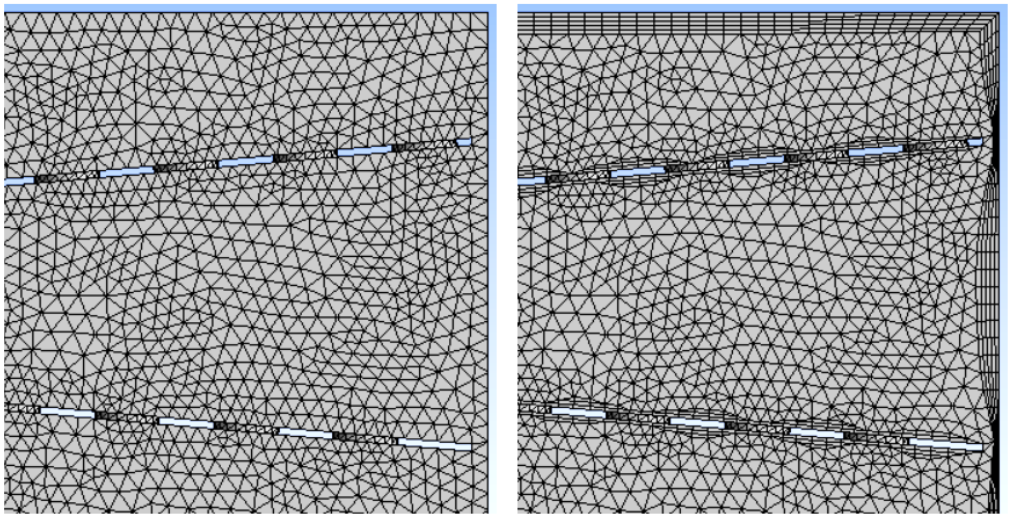

A) Mesh without Inflation layer **B)** Mesh with Inflation layer

Figure 26 - Inflation layer comparison.

Inflation meshing is a proper feature of Ansys Fluent that allows you to create several layers in the normal direction to the boundary until the boundary layer thickness is completely covered.

The physical phenomenon is that the fluid layer within the immediate vicinity of a bounding surface where the consequences of viscosity are significant. The fluids in the boundary layer tend to adhere to the surface, which means that there are velocity gradients within the boundary layer. Obviously, the fluid that is in contact with the boundary will have the same velocity as the boundary, and the velocity of the successive layers of the fluid will increase with a non-linear relation in the velocity profile normal to the direction of the flow.

Within the boundary layer, shear stresses develop between fluid layers that move at different velocities due to viscosity and the interchange of momentum as a result of turbulence. This can cause fluid particles to move from one layer to another.

In applications with highly turbulent flows becomes necessary an accurately capturing these effects at the boundary. In addition to capturing the boundary layer effects, inflation also contributes to a lower element count and computational time [52].

The summary of the meshing data used for the 2nd phase comparison is shown in Table 5.

Mesh data	**Empty Chamber**	**IPP system (5°)**
Type	Tetrahedron	Tetrahedron
Size of element (mm)	20	12
Inflation layer	No	Yes
Number of elements	256892	340018
Skewness	0,83756	0,87852
Orthogonal quality	0,16242	0,12148

Table 5 - Meshing data.

7.2.2 Boundary conditions

For simulations has been used pure water as a fluid because the density of the cultivation medium is very similar to water 1005 kg/m^3 [53]. To monitor hydrodynamic conditions, pure water is the right choice to avoid the waste of microalgae in real experiments. Due to the computational complexity, it is preferable to work only with a single-phase model.

For the first design phase, it has been selected a mass flow rate of $\dot{m}$=1,331 kg/s that corresponds to the 80% of the maximum pump flow rate, to compare all the initial configurations. Knowing the inlet cross-section area, it was possible to calculate the velocity of the inlet flow (Table 6) and for this case is u_{in} = 3,508 m/s.

Case	**Pump**	**Mass flow rate**			**Input nozzle velocity**		
1) Empty chamber 2) Horizzontal IPP 3) 5°-IPP chamber	80%	$\dot{m}$	1,331	kg/s	u_{in}	3,850	m/s

Table 6 - Design phase simulation parameters.

In the sections dedicated to CFD analysis and results for the design phase, the focus was mainly on three configurations: Empty chamber, without any static mixer installed, Horizontal plates in the chamber, and the chamber with 5 degrees IPP system.

Since the aim of the first phase is to find a qualitative geometry, the target data were volume rendering of velocity, streamlines, and vector plots to visualize the movement inside the flat panel, and their discussion was useful to design better the final static mixing solution for this specific case.

Throughout this study, the flow rates of 60, 80, 90% of the maximum available flow rate of the peristaltic pump were taken as reference. Each configuration was analysed with a different velocity scenario since velocity and volumetric flow rate are strictly related to the energy losses in the system but also the quality of the mixing. Each scenario is shown in Table 7.

Setting pump work

Input quality		Low	Mean	High	
Percentage of pump work		60%	80%	90%	
Pump flow rate	$\dot{m}_{pump}$	60	80	90	l/min
		1,000	1,333	1,500	l/s
Mass flow rate	$\dot{m}$	0,998	1,331	1,497	kg/s
Input velocity	u_{in}	2,89	3,85	4,33	m/s

Table 7 - Reference of pumping work for different percentages.

Later, for the 2nd phase, the focus will be only on two configurations: Empty chamber without any static mixer installed and a chamber with 5 degrees IPP system, since the IPP system was chosen for its better hydrodynamic conditions after the studies carried out in the first phase.

Here, it has been added, to the previous parameters, also vortex core region to visualize regions of high energy concentration as vorticity and swirl strength, and also hydraulic parameters as pressure drop will be directly compared.

7.2.3 CFD Simulations

The setup phase was straightforward due to the presence of only one component, water. For boundary conditions, it has been used pressure outlet with pressure at 0 Pa, and mass flow inlet with the three different values (low, mean, high) already shown in Table 7.

It has been performed transient simulation (Fig. 27), which computes the instantaneous values at any time for each quantity so, especially in this turbulent case, it is possible to get better results. A drawback of transient simulation is its high computation time.

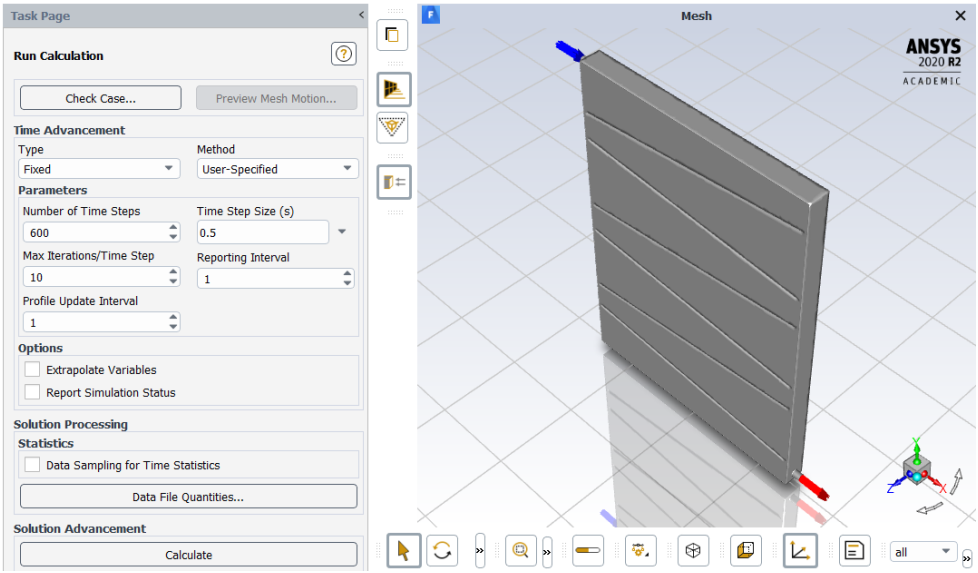

Figure 27 - Ansys extract, setup simulation time.

For the fluid analysis inside the chamber with graphic output such as streamlines, volume rendering and so on, all transient simulations were with 600 timesteps, and each time step was 0,5 seconds and 10 iterations, 3 minutes of working in the reality. But for the study of the residence time and the full homogenization time, the simulations were carried out until the results were obtained.

7.3 Flow analysis

The identification of the flow regime is necessary to understand what the perfect model for simulation is. Usually, to define the flow regime it is used the Reynolds number (Re), which is an indicator of the flow inside a channel, and it is applicable only for fully developed flow.

But obviously, there isn't a proper definition of Reynolds number for a flat panel geometry. Therefore, the only way how to define the Re into a non-homogenous system as is flat panel PBR is to use the CFD simulation.

In FP PBR, it is better to make the distribution of turbulent Reynolds number Re_y [27]. Turbulent Reynolds number [54] is a nondimensional quantity defined as:

$$Re_y = \frac{\rho d\sqrt{k}}{\mu_{lam}} \qquad eq.15$$

Where k is turbulence kinetic energy, d is the distance to the nearest wall, and μ_{lam} is the laminar viscosity.

However, the Re_y can be monitored only in the k-ω model or k-ε model with enhanced wall treatment [55], so after this modification on the CFD model, It has been possible to estimate Re_y, and visualize it thanks to a proper contour (Fig. 28).

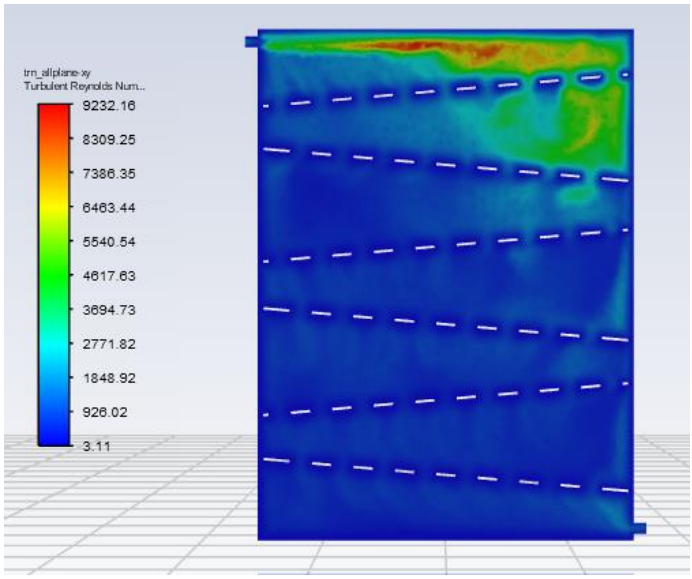

Figure 28 - Turbulent Reynolds number distribution on plane Y-X.

It has been calculated the mean turbulent Reynolds number on all plane Y-X, and to better understand the situation inside the chamber, two clipped surfaces were created, where it was possible to calculate the mean Re_y on the upper and lower part of the chamber, they are defined as, respectively, 30% of the length from the top and 30% from the bottom.

Since the definition of the boundary for the laminar, transient, and the turbulent regime is still valid, Laminar flow occurs when Re < 2300. According to the simulation, it is possible to observe the decrease of Re from the top area of the chamber to the bottom one (Fig. 28, 29).

Turbulent Reynolds Number (Re_y)	
down-clip	627.50094
plane-yx	3027.0045
up-clip	3848.3101

Figure 29 - Mean turbulent Reynolds distribution.

These data, as shown in the CFD result part, are well harmonized with all other calculated parameters as velocity contours, swirl strength, and vorticity shown below.

7.4 CFD results

Each following configuration has been achieved a good convergence of the results (Fig. 30). Convergence is a universal concept in finite element analysis. If a model contains non-linearity, it cannot be solved directly, so it must be found the solution by iteration. Although you cannot find an exact solution, the convergence criterion defines how close the approximate solution found is to the real value [41].

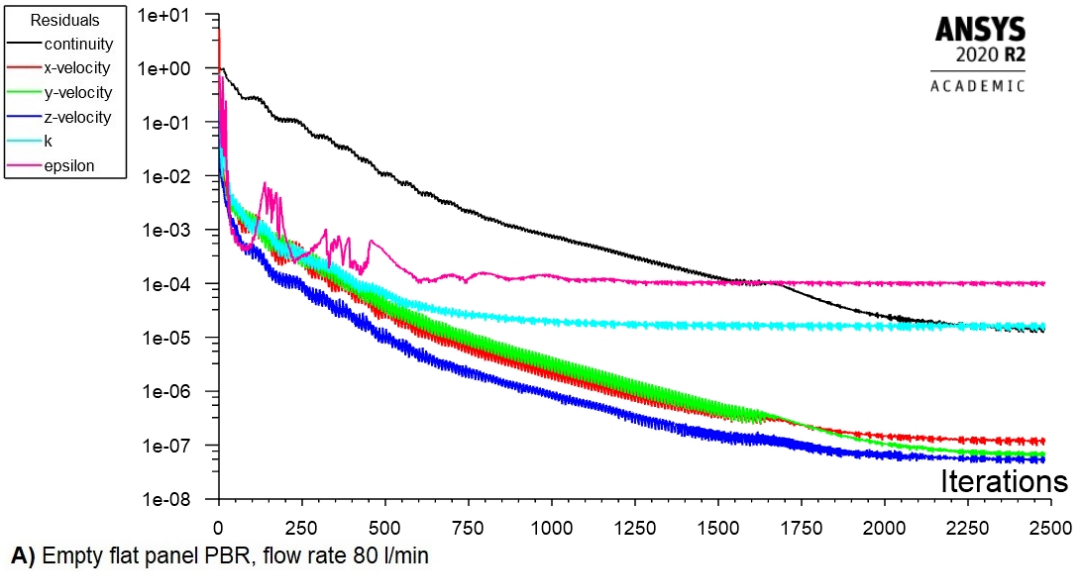

A) Empty flat panel PBR, flow rate 80 l/min

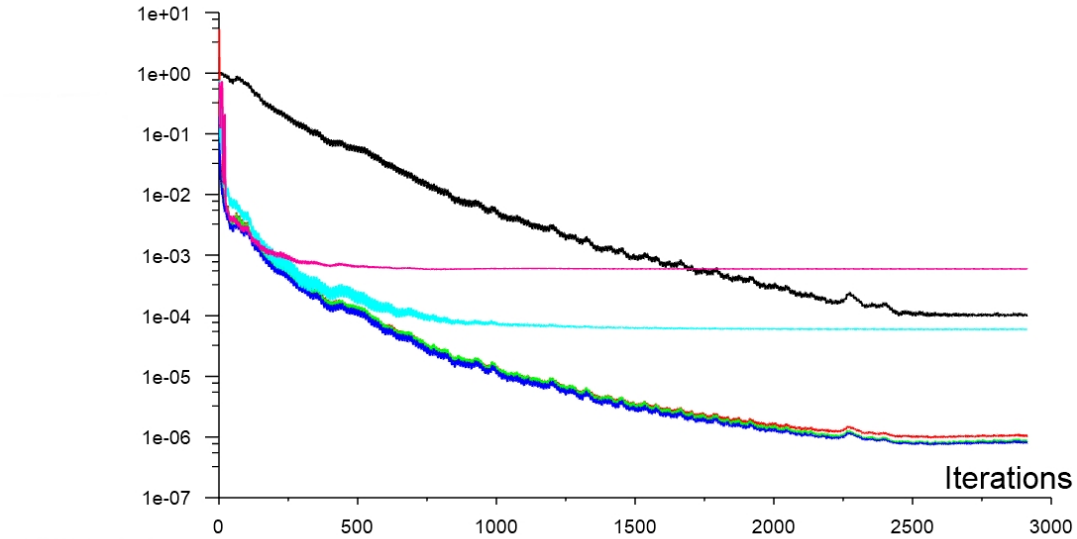

B) Flat panel PBR with IPP system installed, flow rate 80 l/min

Figure 30 - Residuals graphic outputs.

During a simulation, the residuals should decrease towards zero, and a common practice is to stop the simulations at a certain threshold value. If the residuals in a

simulation do not decrease but fluctuate around a relatively high value, the solver was unable to find a solution with the current model configuration.

There are three indicators that convergence has been reached [56]:

1. The residuals have decreased to a sufficient degree.
2. The solution no longer changes with more iterations.
3. The overall mass and momentum balances are obtained.

All the simulations were carried out using a transient solver with the first-order implicit scheme in transient formulation, and as under-relaxation factors, 0,2 for pressure and 0,8 for momentum were used to achieve the convergence. In solution methods setup, it has been chosen for the empty chamber configuration, as spatial discretization, the second-order calculation for the pressure, but for the chamber with IPP system installed, where the problem was harder to solve, it was used the standard method.

In Fig. 30 are reported the residuals output graphs for the main 2 configurations simulated: Empty flat panel PBR, and Flat panel PBR with IPP system installed, both with 80 l/min as a flowrate.

For each configuration tested, the convergence criterion for each variable has been reached; and after a certain number of iterations, the residuals reach a stable value well below 10^{-3} (The default criterion is that each residual has to be reduced to a value of less than 10^{-3} [56]), and also the overall mass balances were always obtained.

7.4.1 Design phase

Thanks to velocity volume rendering, streamlines, and vector plots, it was possible to have an excellent description of the fluid flow and how it behaved inside the chamber. The simulations reflect what was thought, and they were useful to improve the first designed configuration with the horizontal plate.

In the empty configuration (Fig. 31 A), without any static mixer installed, a motion is established on the walls of the chamber, which are unable to guarantee a

homogeneous mix in the central part of the chamber, thus limiting the growth of microalgae in the chamber.

Thanks to the streamlines, it was also possible to detect a probable phenomenon of unwanted backflow that occurs in the first stage of the configuration with horizontal plates (Fig. 31 B).

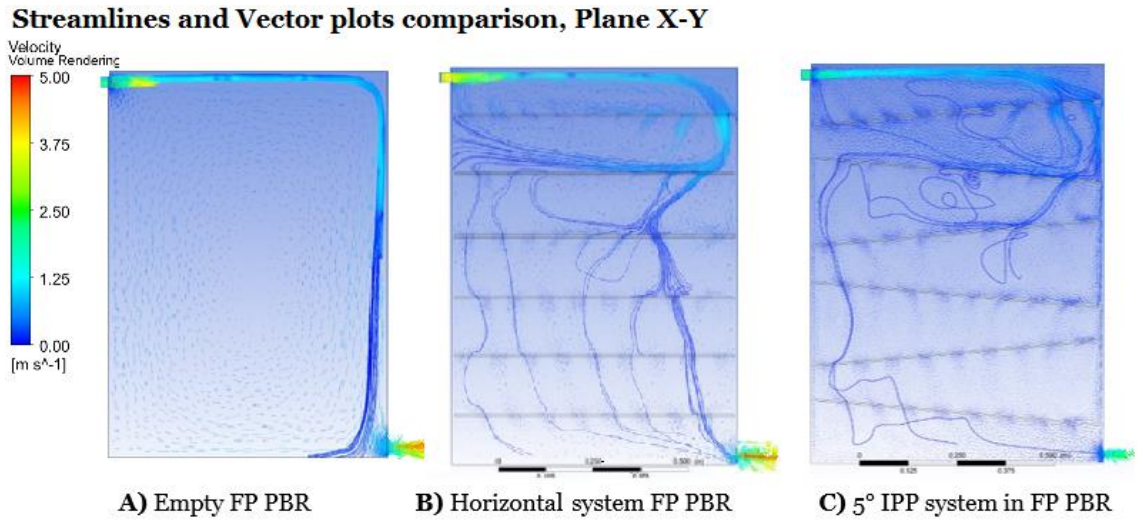

Figure 31 - Design phase: Streamlines and velocity vector plot comparison.

Instead, the difference is clearly noticeable when the IPP System is installed, even in a horizontal configuration is possible to see how the flow assumes an obligatory sinusoidal path (Fig. 31 B, C). Moreover, the IPP system configuration significantly reduces the backflows, and it allows the best distribution throughout the entire volume of the chamber.

The choice of tilting the plates to better intercept the initial flow and avoid sedimentation was confirmed by the simulations (Fig. 32).

Furthermore, this configuration would seem to generate much more turbulence in all areas where the distance between the plates is wider (Fig. 32 C), creating narrow vortexes, compared to when the plates were arranged horizontally, and the flow followed a more "standard" path.

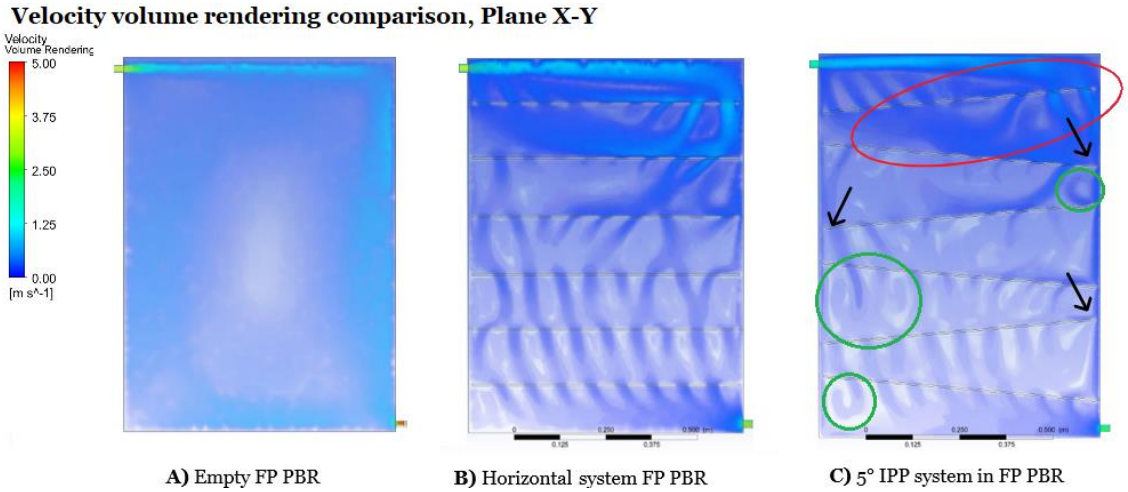

Figure 32 - Design phase: Velocity volume rendering comparison.

The 5° degrees IPP System was chosen as a final configuration, which was also used for a direct comparison with the Empty chamber. In the next section, these configurations have been explored by also analysing the vortex core region to visualize regions of high energy concentration as vorticity and swirl strength, residence time and the pressure drop with different flow rates was also investigated.

7.4.2 Empty chamber vs IPP system

To better understand the characteristics of this static mixing system, it may also be helpful to compare it with for empty chamber directly. The IPP system was able to distribute and homogenize the input flow. Fig. 33 B shows how the energy, represented by the velocity of the fluid, is dissipated during its path. The static perforated plates intercept the fluid and direct it in the whole volume of the chamber.

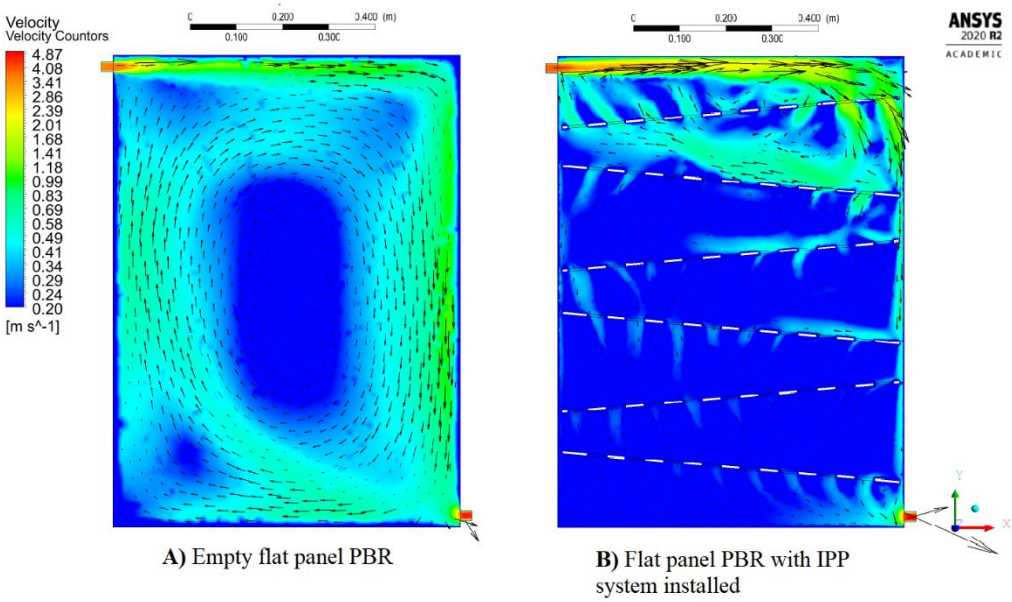

Figure 33 - Comparison between Empty chamber (A) and chamber with IPP 5° (B). Countors of velocity and vector. Flow rate 80 l/min.

But the most important thing is that when the IPP is installed, the first stage absorbs almost all the energy of the fluid, and this could guarantee and confirm the light mixing hypothesis explained above, therefore less dissipation and energy losses.

In fact, a high turbulent regime can damage the microalgae organism, and it is not always indicative of a better homogenization; moreover, the turbulent flow has a high dissipative state, and since this work aims to achieve the economic feasibility of the microalgae production due to a better homogenization to increase the growth, is also important to take into account the energy losses during the entire process.

In the following Fig. 34, on the left, is shown the velocity contour in logarithmic scale to better highlight the fluid flow with lower velocities.

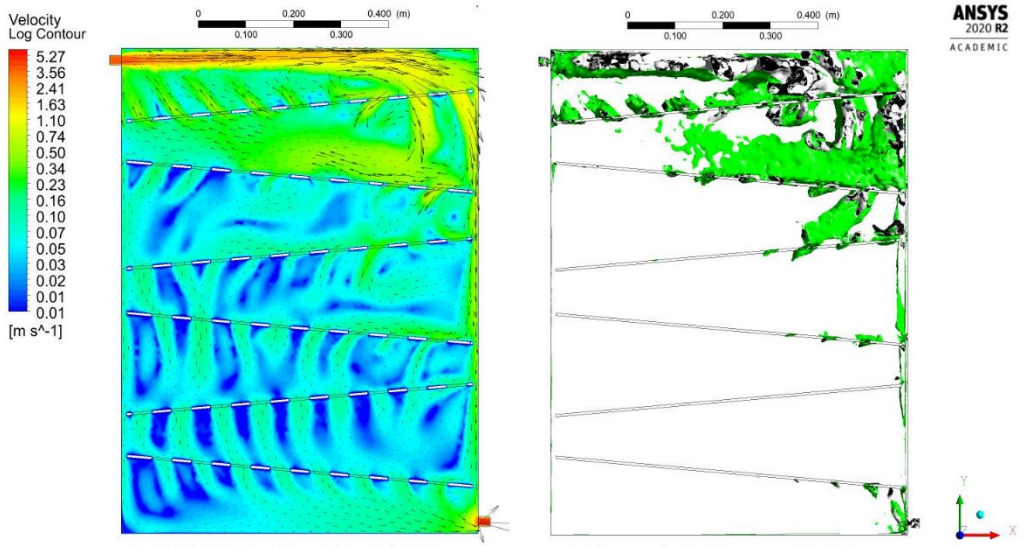

A) Flat panel with IPP system. Velocity contour, logarithmic scale.

B) Flat panel with IPP system. Vorticity (Green), Swirl strenght (Gray)

Figure 34 - IPP system, flowrate 80 l/m. Velocity contour in logarithmic scale and vortex core regions.

It is easy to see that, thanks to the IPP system, the stagnant zones inside the chamber are minimized, and it is no more present the big centre spot of steady fluid that was present in the empty chamber. It will be shown later, with the volume rendering, that this characteristic is also maintained with different flow rates.

This arrangement was able to create a forced pathway around the chamber that can spread and homogenize the microalgae culture in all the volume allowing a better distribution of nutrients, temperature, and light.

In Fig. 34 B are shown the vorticity and the swirl strength vortex core regions, they are parameters that allow to determine the turbulence within a fluid and visualize the regions of high energy concentration; as explained before, the first one is a pseudovector field that describes the local spinning motion of a continuum near some point (the tendency of something to rotate), and the swirl strength represents the strength and the density of the local swirling motion.

As easily predictable, the highest energy zone is the one in which the fluid is forced to change direction, therefore at the end of the chamber, with the IPP system, the first plate is inclined to better intercept this direction change, but this arrangement causes an even greater "stress" on the fluid as there is less free space.

Fig. 35 shown how the IPP system reacts with different flow rates. These analyses were useful to understand the disadvantages of this system.

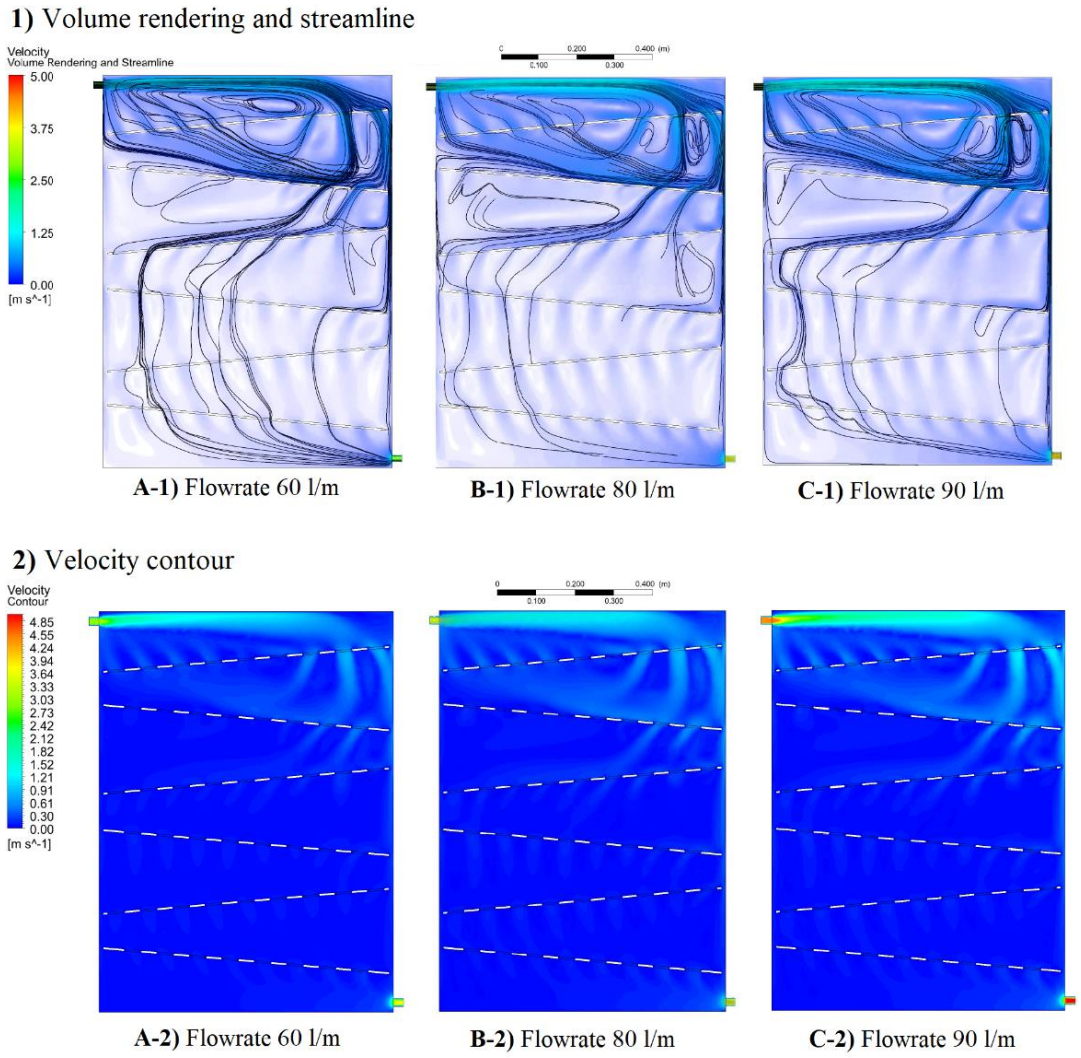

Figure 35 - IPP system at different flow rates. Volume rendering and streamline, Velocity contour.

During these CFD analyses, the streamlines were useful to visualize the fluid pathway and, two main drawbacks were observed, a significant backflow in the top of the chamber and the presence of an unmixed lateral flow.

After the first perforated plate, the fluid flow impacts the closed space on the second plate and starts to rotate back, and a circular movement is established in the first 2 stages, powered by the incoming flow. This effect was not desired, however, a high energy zone (Fig. 35 B) is created in this upper area of the chamber, which ensures good mixing, but this situation was not too necessary and could be a waste of energy.

As shown in Fig. 35 A, a different flow rate cannot change this situation, but a lower flow rate (Fig 35 B) decreases the velocity of the backflows, allowing for more delicate mixing.

The worst problem encountered is the formation of an unmixed lateral flow into the drainage space that was intended to limit sedimentation. This effect can be problematic because it allows the input stream to totally bypass the entire static mixer and go straight to the output. Also, in this case, it was tried to act on the input flow rate, but the problem persists.

The only way to eliminate this unmixed flow is to act directly on the geometry of the static mixer or by introducing some elements to influence the movement of the flows inside the chamber. Further analysis will be needed to estimate the real amount of unmixed microalgae and whether that amount really affects the total homogenization. A possible solution to these problems will then be presented.

To deepen the analysis of both configurations, some specific simulations were carried out to determine the dynamic nature of the problem under consideration.

For both configurations, a non-reactive tracer with the same fluid dynamics characteristics of the bulk fluid was used in order to study the residence time and the homogenization time. These simulations were carried out for the “Mean” case (Table 8), so with a flow rate of 80 l/min. But a further extreme check was also carried out with a flow rate of 40 l/min.

Residence time analysis

In this thesis, where the aim was also to design an effective mixing system for a flat panel PBR, the study of the residence time itself, used as a pure time of a fluid in a given control volume, is not properly indicative of the quality of mixing and homogenization. However, its analysis, contextualized to this case study, can provide very useful information on the effectiveness of the IPP system compared to the empty chamber. Moreover, the residence time is important for microalgae cultivation since they need to be irradiated by the light source for a certain amount of time. These time measurements can also be used as a future validation, by laboratory experiments, of the mathematical model created.

The residence time analysis was carried out by tracing the mass fraction of the incoming tracer in 7 different control points, represented in Fig. 36, so it was possible to map the entire volume, obtaining more reliable data and a greater understanding of the situation, in fact, especially in the case of the empty chamber, the mere use of the input and output control points would have led to misleading results, since, as already shown in the previous section, the central area in the empty chamber is characterized by a significant dead zone without mixing, as the flow flows against the walls quickly reaching the output nozzle.

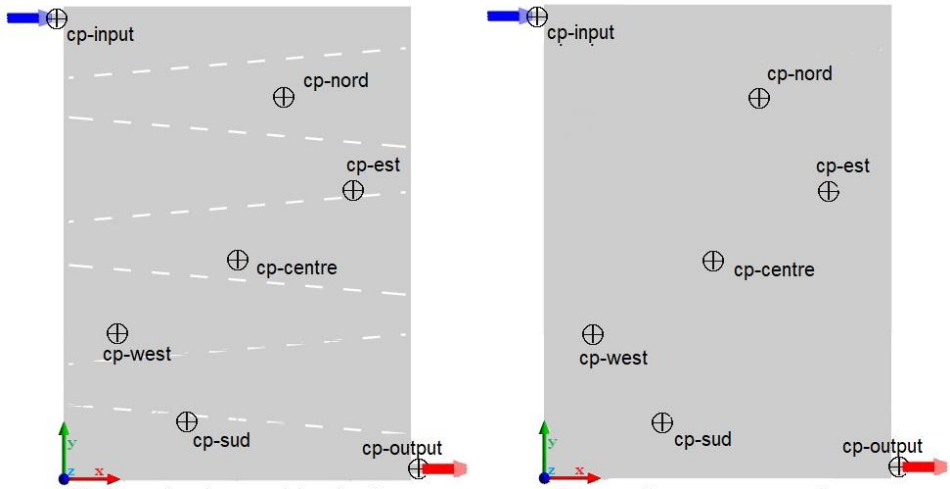

A) Control points position for flat panel PBR with IPP system.

B) Control points position for empty flat panel PBR.

Figure 36 - Control points for residence time analysis.

The inlet and outlet control points have been inserted directly into their respective nozzles, so they were not affected by secondary flows inside the chamber.

Taking the lower left angle of the chamber as the origin, Table 8 shows the geometric coordinates of the various control points.

Control points

	x [mm]	y [mm]	z [mm]
cp_Input	-15	1000	32,5
cp_nord	500	860	32,5
cp_est	650	650	32,5
cp_centre	375	510	32,5
cp_west	100	370	32,5
cp_sud	250	160	32,5
cp_output	765	20	32,5

Table 8 - Geometric coordinates of the control points.

From the instant **t = 0** sec. to **t = 50** sec. a tracer was continuously injected, after stopping the injection of the tracer, the simulation was continued by introducing the bulk fluid into the chamber for a relatively long time to obtain reasonable results.

Both chambers are filled with bulk fluid (water) in the initial moment, and when the simulation begins, the non-reactive tracer is immediately introduced. As shown in Fig. 37, the tracer propagates inside the chambers, reflecting what was hypothesized with the study of the volume rendering and streamlines (Fig. 33). Already at the instant **t = 25** sec. (Fig. 37-B) the flow assumes a circulatory movement against the walls of the empty chamber. After 50 seconds of continuous injection of the tracer, the simulation was continued by introducing only the bulk fluid in order to determine how long it took to eliminate the presence of the tracer inside the chamber.

Fig. 37, last instant shown at **t = 100** sec. anticipates how, in the case of the flat panel PBR with the IPP system installed, the tracer has been homogeneously "swept away" from top to bottom, while in the empty flat panel PBR, the circulatory flow is established and it "blocks" the mass of the tracer present in the central area, making this system unsuitable for complete homogenization.

In Fig. 37, the contours of the mass fraction of the tracer of the main steps have been reported.

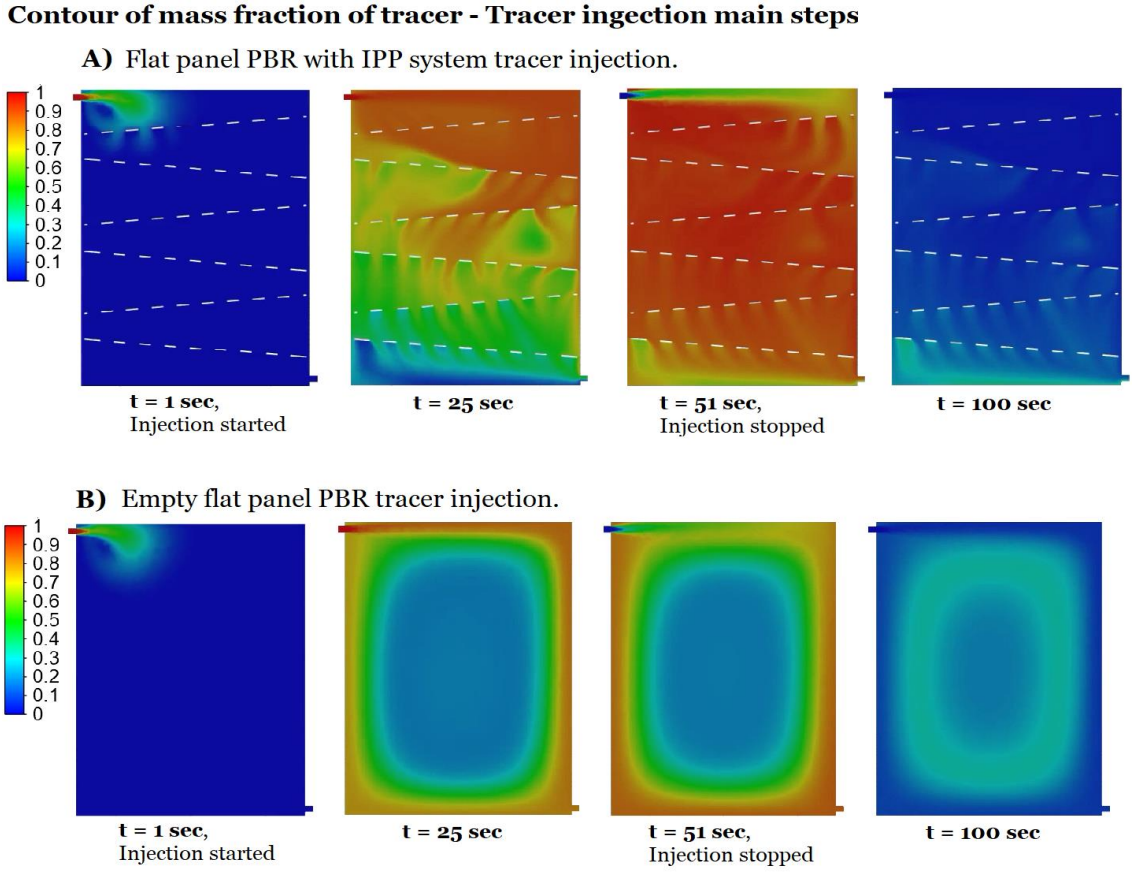

Figure 37 - Contours of mass fraction tracers during operations.

Fig. 38 shows the graphs with the detected data from the control points. For both graphs, the red curve represents the tracer mass fraction measured from the control point in the inlet nozzle, the black curve represents the tracer mass fraction in the outlet nozzle, while the others are representative of the other points of control. Fig. 38 refers to a flow rate of 80 l/min.

In the flat panel PBR with IPP system, the mass fraction grows uniformly in all the control points. The control points located in the lower part of the chamber have a slight delay given by the type of propagation from top to bottom, also shown in Fig. 37.

Furthermore, for the representative curves of the North and East control points (yellow and green curves in Fig. 38 A), a minor irregularity in the first instants of operation was formed, this was because the first 2 plates absorb the energy of the

incoming flow and they are intended to change the circulatory nature that fluid would have in a flat panel PBR without any mixing system, and therefore these two control points, in the first moments, are subject to small reflux phenomena.

Once the tracer injection is finished, at the instant **t = 50** sec., the inlet control point obviously begins to detect only the incoming bulk fluid, so the red curve suddenly decreases, as a typical step function.

Also, when the IPP system is installed in the flat panel PBR, the tracer discharging phase is characterized by a uniform descent of the tracer mass fraction in all control points. Approximately after 160 seconds from the beginning of the operation, all the control points no longer detect the presence of the tracer inside the chamber.

At **t = 50** sec., in Fig. 38 A, all the control points record very high and uniform mass fraction values of the tracer, greater than 80%. This phenomenon is representative of the rapid diffusion of the tracer inside the chamber, obviously, this also depends on the inlet flow rate and the volume of the chamber, in fact, the values reached in the case reported below (Fig. 39) are lower. But, for each flow rate tested (40 and 80 l/min), the analysis carried, show that the mass fraction reached with the empty chamber is significantly lower than the one reached with the IPP system installed (Fig. 38, Fig. 39).

As regards the empty chamber, the deviation of the mass fraction measured at the outlet with that measured by the other control points is very relevant (Fig. 38 B), for this reason, the study with only 2 control points at the inlet and the outlet it would have been misleading.

In the injection phase of the tracer, it is evident how the central areas of the empty chamber receive only a small portion of the incoming mass, and as shown in Fig. 37 B, **t = 25** sec., the input flow flows adjacent to the walls until it immediately reaches the output. This is also represented by the rapid rise of the mass fraction detected by the output control point (Fig. 38 B).

The significant difference in the mass fraction values, in the different control points, detected during the entire operating phase is an indicator of the poor homogenization that the empty chamber can offer.

Analysing the tracer discharging phase, is it possible to see a rapid descent of the mass fraction measured at the output, which as for the tracer injection phase, indicates that the incoming fluid reaches the exit directly, making it almost useless to pass through the chamber itself.

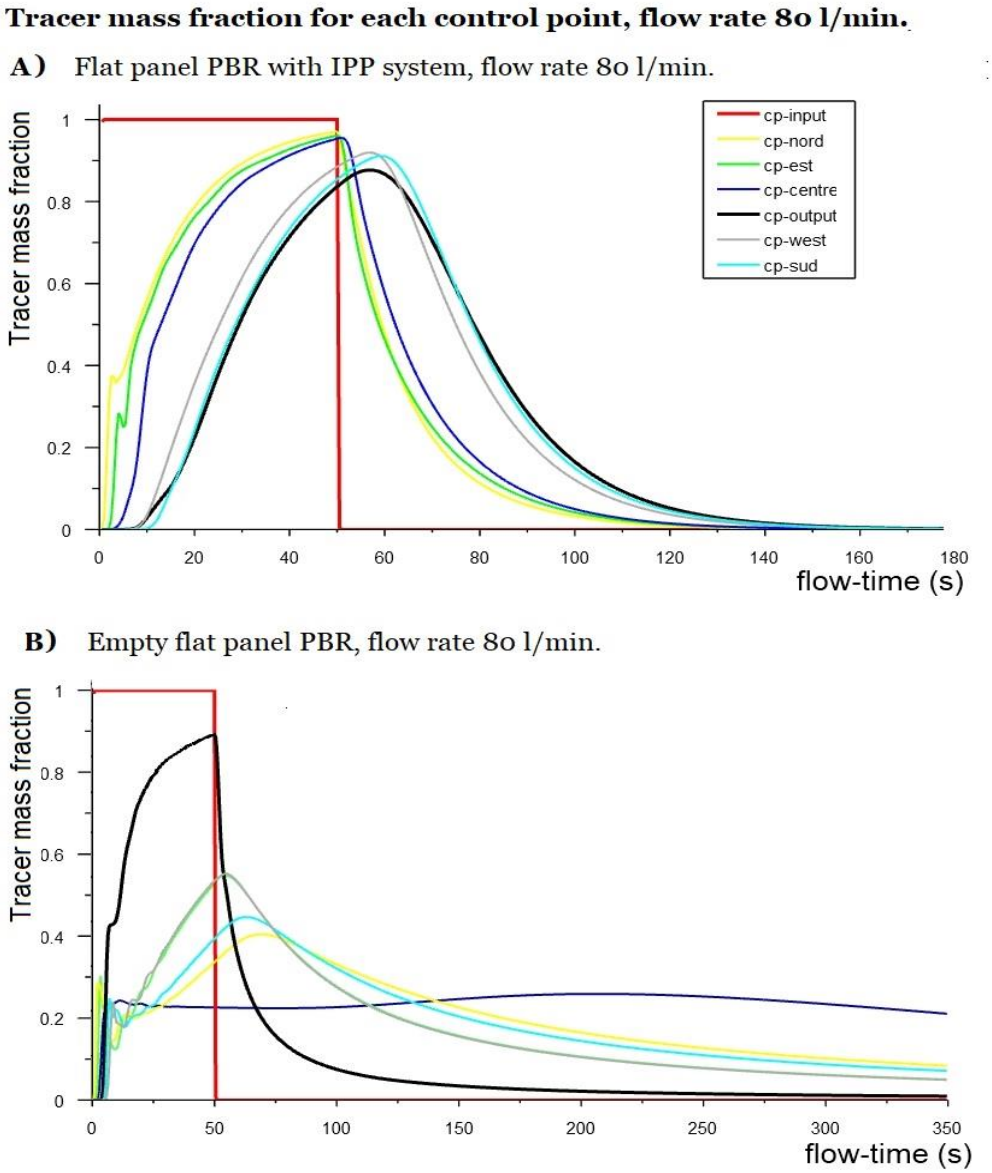

Figure 38 - Mass fraction of tracer for each control point in time flow. Flow rate 80 l/min.

The other curves in the graph in Fig. 38 B show a long residence time, which represents a strong inability of the empty chamber to "dilute" the tracer present in the chamber volume, and therefore a poor mixing power, in fact, thanks to the qualitative analysis shown previously, it is known that these stable mass fraction values are given by the stagnant tracer in the central area of the flat panel PBR, which is slowly reduced during the continuous operation, described by the slow

descent of the mass fraction values detected by the peripheral control points in the central area represented by the curves in Fig. 38 B.

As the inlet flow increases, the formation of the circulatory flow adjacent to the walls is amplified, and this flow could more block the outflow of the tracer “trapped” in the central area. A drastic test was performed, halving the inlet flow, setting it to 40 l/min. Furthermore, this test was useful to test the IPP system in unfavourable conditions. In Fig. 39, the results of this simulation are shown, and, as anticipated, the measured mass fraction values are slightly lower.

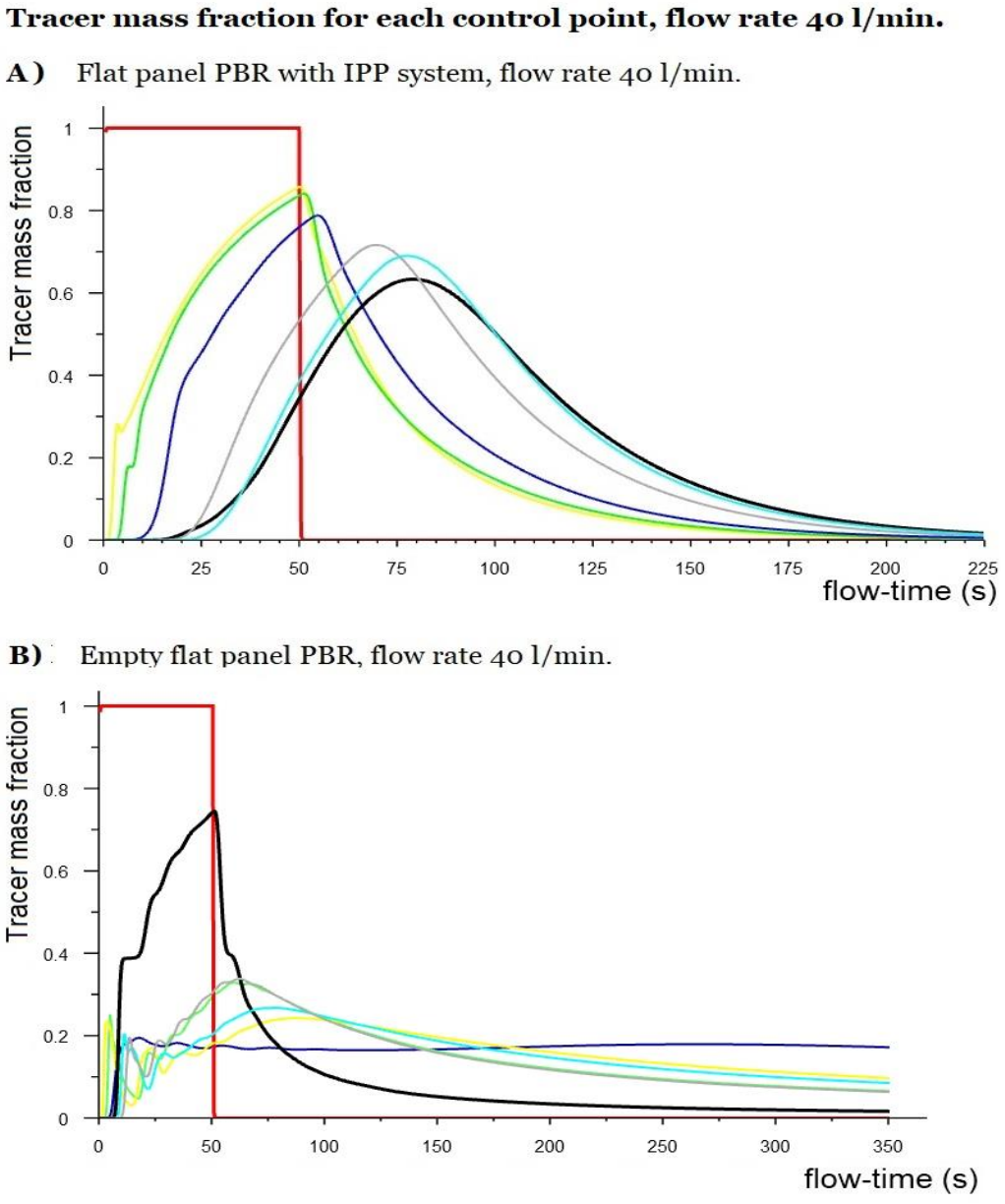

Figure 39 - Mass fraction of tracer for each control point in time flow. Flow rate 40 l/min.

For both cases, no difference was obtained, in fact, all the phenomena described above recur even with a considerably lower flow rate. This result shows an effective inability to homogenize for the empty chamber but an excellent result for the IPP system, which is, therefore, able to work at lower flow rates without losing its mixing power. Obviously, by also reducing the flow rate of the bulk fluid, the residence time increases.

Homogenization time

Another characteristic parameter of the problem treated, is the total homogenization time, or the ability to distribute the fluid inside the entire volume of a reactor. The shorter the homogenization time, the better the system. To measure the homogenization time, the most problematic death zone for each configuration was identified, and a control point was inserted in that position. For the flat panel with the IPP system, the identified death zone is immediately under the last plate on the left (Fig. 40 A), while for the empty chamber, it was the already known central point.

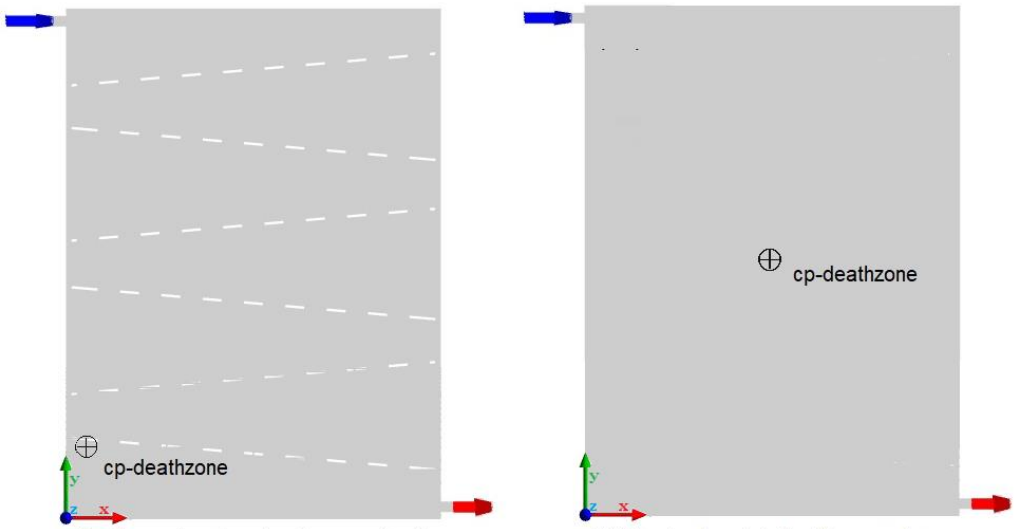

A) Control point death zone for flat panel PBR with IPP system.

B) Control point death zone for empty flat panel PBR.

Figure 40 - Control points for homogenization time.

The whole volume of the flat panel was initialized full of bulk fluid, but the inlet flow rate was made up of only tracers with a flow rate of 80 l/min for both configurations.

The simulations performed until the mass fraction detection from the control point located in the death zone, reach the value of 1, so when even in the most difficult

area to reach, 100% of tracer was obtained, thus indicate that a full homogenization has been obtained.

Fig. 41 shows the trends of the values detected by the control points. For the flat panel with the IPP system, the complete homogenization was obtained around 120 seconds, while obtaining a homogenization of 80% took only about 60 seconds. As for the empty chamber, 80% homogenization was achieved after 600 seconds, and a time greater than 1200 seconds (20 minutes) was required for complete homogenization.

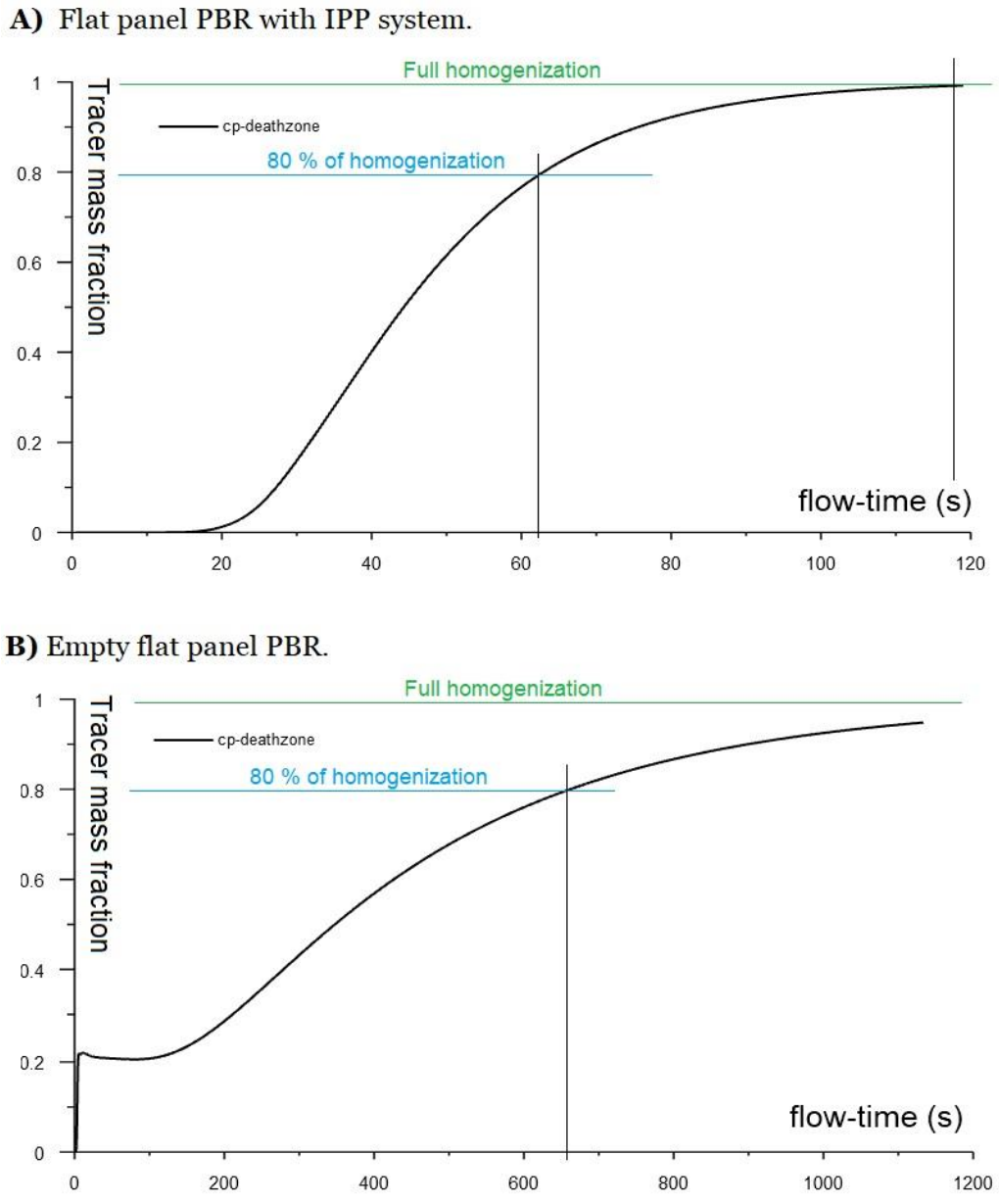

Figure 41 - Mass fraction of tracer to detect homogenization time.

These last two parameters obtained and the analysis carried out on the values detected by the different control points are the most indicative results regarding the capacity of mixing and homogeneous distribution of the fluid in the two systems examined, empty flat panel and flat panel with IPP system.

For evaluation of homogenization, the hydraulic retention time (HRT) was also taken into account, where HRT is the volume of the flat panel PBR chamber divided by the influent flow rate. In case of the IPP system, the volume of the plates was assumed negligible compared to the volume of the chamber (V_{plates} = 0,001 m^3).

It has been compared the full homogenization time with the hydraulic retention time in Table 11, it is evident, for both configurations, that the homogenization time is longer than the hydraulic retention time. This difference is caused by the formation of stagnant areas in the flat panel PBR chamber, in fact, in the empty chamber, where the central death zone is much bigger than the death zone in the chamber with IPP sys installed, the difference between homogenization time and HRT is higher.

Table 9 summarizes all the obtained values for the tracer injection simulations.

Residence time and Homogenization time

Parameter	IPP sys + FP PBR		Empty FP PBR	
Flow rate (l/min)	40	80	40	80
HRT (s)	75	37	75	37
RT (s)	130	175	>> 300	>> 300
Full homogenization time (s)	250	120	>2000	> 1200
Homogenization time (80 %) (s)	125	62	900	660

Table 9 - Residence time and homogenization time

Pressure drops

Since it has been spoken about energy losses and light mixing idea, to challenge this previous hypothesis, it has been calculated the pressure drops ΔP [kPa], between input and output of the chamber, in both configurations, for each flow rates, $\dot{m}$ [kg/s] (Table 10):

Pressure drop

Pump	Mass flow rate	Input velocity	Empty chamber	IPP system	IPP losses
	ṁ [kg/s]	u_{in} [m/s]	ΔP [kPa]	ΔP [kPa]	Δ [kPa]
60%	0,998	2,887	7,155	7,935	0,780
80%	1,331	3,850	13,427	14,566	1,139
90%	1,497	4,331	17,447	18,957	1,510

Table 10 - Pressure drop difference.

The pressure losses due to the installation of this type of static mixer, with the plate inclined by 5 degrees, are around 1 kPa, and obviously, the pressure losses increase with the total velocity. The IPP System with 5 degrees tilted plates ensures a qualitative homogenization, which is clearly better than the empty configuration. The sinusoidal pathway that the flow assumes in the chamber could guarantee a powerful distribution around the chamber with less energy utilization.

7.4.3 Deflector cap

For further optimization of the technology, an additional component has been designed. It can be inserted in any area of the flat panel, this could guarantee the dynamic direct correction of the fluid motion, where necessary, by acting locally. The purpose of this component is to extend the working range in order to maximize homogenization for each type of flow, therefore, for each type of situation.

The component is a 3D printable deflector cap. It has been designed to be easily attached and detached in any position corresponding to a hole in the plates, using three simple supports with a groove of the same diameter as the holes (Fig. 42).

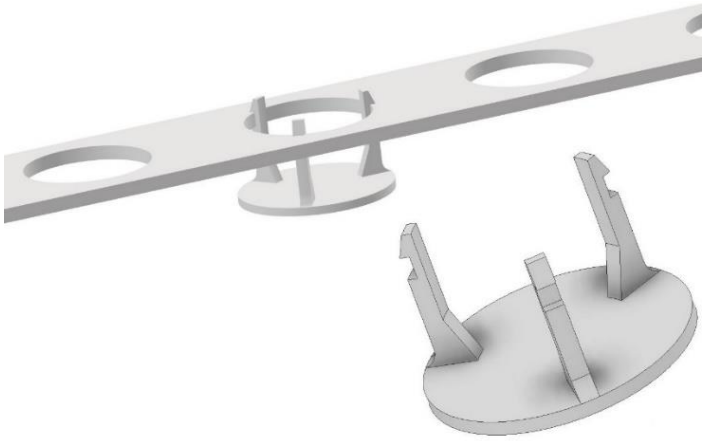

Figure 42 - Deflector cap design.

As was shown in the discussion results section, some undesirable effects were highlighted, some anomalies that could affect the quality of homogenization, it was shown that they also varied according to the flow rate entering the flat panel.

Some simulations were then carried out to understand if the Deflector caps could eliminate these effects. The purpose of this component, in fact, is to locally alter the motion of the fluid when it is not possible to change the flow rate.

As shown in Fig. 43 B, two deflector caps were inserted in the first stage, and a comparison was made with 80% of the inlet flow. The first deflector cap placed on the right was able to deflect and distribute the flow, modifying the main fluid dynamics, which allowed to disturb and therefore reduce the problem of unmixed lateral flow. The second deflector cap inserted centrally in the chamber was able to

limit the backflow problem, and the fluid was partially conveyed in the desired direction (Fig. 43 B).

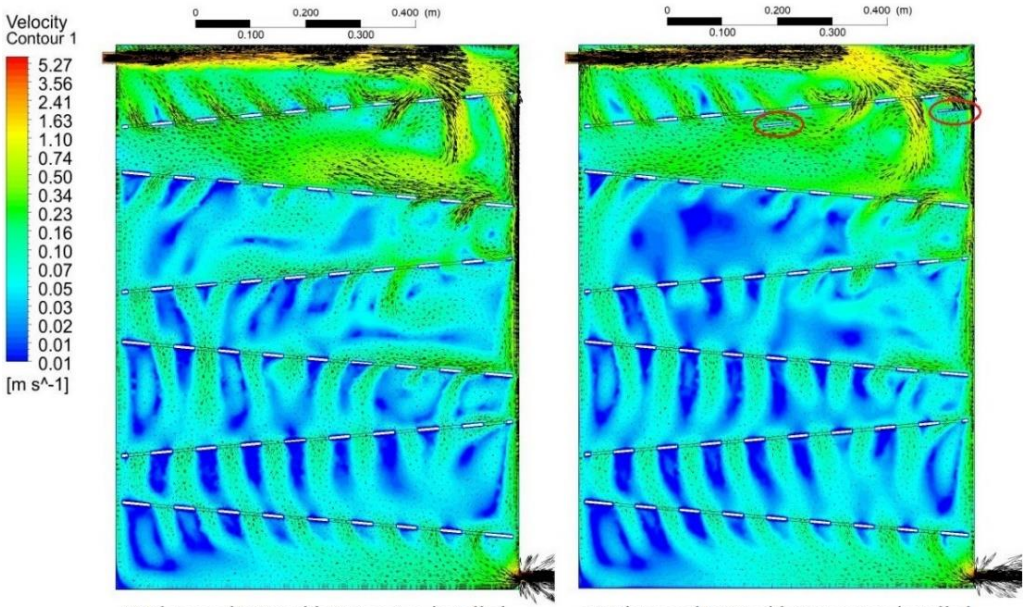

Figure 43 - Comparison by velocity countors and vector plot after deflector plate installation. Flow rate 80 l/min. Logarithmic scale.

Therefore, this component has proved useful, if correctly placed, to widen the diffusion of the flow, decrease the formation of the unmixed lateral flow, moreover it could be able to reduce the reflux phenomenon.

This prototyping is only in the first step of the hydrodynamic study, it would be necessary to verify the mechanical strength and the manufacturing technique of the deflector cap, but these simulations, together with the probably negligible production cost, and the high adaptability since this component can be placed anywhere, show that further investigations on this deflector cap make sense.

Chapter 8
CONCLUSION

This document contains some theoretical background, analysis and simulations of the 2 main phases of this engineering work: design and simulation phase. This work intentionally follows the scheme described in the "strategy of work " chapter because the goal was to explain the true line of thinking behind creating something new, with all the trials and errors made.

For the first design phase, all the work instructions are described, with the ideas behind the chosen geometry, and with all the CFD simulations that led to the exclusion of some geometries rather than others.

The mathematical analysis and the creation of a "virtual" model, thanks to the Fluent Ansys software, was the central part of this work, and it was essential for the study of the hydrodynamic conditions of the PBR flat panel used. This modelling allowed an a priori study of an ideal configuration which can then be actually built.

The final aim was to find an efficient and inexpensive static mixing system to improve microalgae growth and production of biomass.

The Inclined Perforated Plate (IPP) System is the solution presented in this work, a new concept of static mixing system, where, thanks to the best and favourable hydrodynamic conditions inside the chamber, it is able to maximize the interaction with all nutrients and CO_2 necessary for the growth of microalgae and can keep all the cells in suspension with free access to light. It can also prevent the biomass from sedimentation and aggregation, improving mass transfer and eliminating light gradients.

It was also highlighted how, compared to the empty chamber, without any static mixer installed, where it was not possible to guarantee a homogeneous mixing in the central part of the chamber, the IPP system was able to create the best distribution

over the entire volume of the chamber thanks to the obligatory sinusoidal path forced by this arrangement of the plates.

This IPP system has a minimal surface area in the normal light impact direction, so it optimizes light transmission between the source and the microalgae as it does not block the incoming light. This, in the production reality, translates into maximum transmission capacity and transmission efficiency, therefore less energy wasted.

The inclined arrangement of the plates significantly avoids the sedimentation phenomenon (thanks also to the minimum roughness of the chosen material), and thanks to the small gap between the plates and the wall, the microalgae culture can easily "drainage".

However, this geometry presents 2 main disadvantages: a backflow phenomenon in the first stage and the formation of an unmixed lateral flow. As presented before, the backflow phenomenon is established due to the incoming flow, from the input nozzle, at the top of the flat panel PBR, when the flow enters, it assumes a very precise boundary, and it must be intercepted to ensure excellent mixing from the top of the flat panel. The first inclined plate performs this task very well. The unmixed lateral flow is irrelevant compared to the circulatory movement of the fluid in an empty chamber.

The simulations with a non-reactive tracer have been shown the real effectiveness of the IPP system. A uniform trend of the monitored data by the control points has been achieved, therefore the composition inside a flat panel PBR with IPP system installed, is homogeneous, highly responsive, and it is possible to achieve the full homogenization of the whole chamber in only 120 seconds of operation, a significantly lower value than the one needed in an empty chamber (more than 1200s).

The simple geometry designed allows less aggressive mixing that could minimize damage to microalgae with a consequent improvement in quality and quantity of the produced biomass, and, first of all, it guarantees low pressure losses. It has been shown the high performance of the IPP system also with lower flow rate. Thanks to the lower pressure losses and all the above mentioned features, this static mixing

system could make the process more economically feasible than a standard empty chamber of a flat panel PBR.

The IPP system was designed, and in-depth analyses were carried out on it. According to the simulations, with this geometry, it would be possible to obtain a greater homogenization of the microalgae culture throughout the volume of the chamber, maximizing growth but minimizing energy losses, also in reality.

The topic under consideration is well harmonized with the current situation in which the microalgae represents a really interesting feedstock for industries from food to pharmaceutical and also for fuel production, but today, the production of microalgae is not always economically feasible.

NOTATIONS

a	width of rectangular channel [m]
b	height side of rectangular channel [m]
$C(t)$	instant concentration [kg/m3]
CFD	computational fluid dynamics
C_{max}	tracer concentration input [kg/m3]
C_{step}	tracer concentration output [kg/m3]
d	distance to the nearest wall [m]
D_e	equivalent (hydraulic) diameter [m]
D_n	nozzle diameter [m]
$F(t)$	cumulative residence time distribution
FP	flat panel
g	gravitational force [m/s2]
G_b	buoyancy generation of turbulence kinetic energy
G_k	velocity grad. generation of turb. kinetic energy
H	internal chamber height [m]
HRT	hydraulic retention time [s]
IPP	inclined perforated plates
k	turbulence kinetic energy
L	internal chamber width [m]
$\dot{m}$	mass flowrate [kg/s]
$\dot{m}_{pump}$	mass flowrate [l/min]
$\dot{n}$	volumetric flowrate [l/min]
PBR	photobioreactor
Re_y	turbulent Reynolds number
RT	residence time [s]

RTD	Residence time distribution [s]
R_{ij}	Reynolds stress tensor
Re	Reynolds number
S	internal chamber depth [m]
$\bar{u}$	mean velocity [m/s]
u'	fluctuating velocity [m/s]
u_{in}	mean velocity at inlet nozzle [m/s]
$\vec{u}$	vector of instant velocity [m/s]
∇p	pressure gradient
V	chamber volume [m3]
V_{plates}	IPP plates volume [m3]
$\dot{V}$	volumetric flowrate [m3/s]
Y_m	fluctuating dilatation turbulence
μ	dynamic viscosity [pa s]
μ_{lam}	laminar viscosity
μ_t	turbulent viscosity
μ_w	dynamic viscosity of water [pa s]
ρ	density [kg/m3]
ρ_w	density of water [kg/m3]
σ_k	turbulent Prandtl numbers for k
σ_ε	turbulent Prandtl numbers for ε

BIBLIOGRAPHY

[1] R. Ramanan, B. H. Kim, D. H. Cho, H. M. Oh, and H. S. Kim, "Algae-bacteria interactions: Evolution, ecology and emerging applications," *Biotechnology Advances*, vol. 34, no. 1. Elsevier Inc., pp. 14–29, Jan. 01, 2016, doi: 10.1016/j.biotechadv.2015.12.003.

[2] R. Slade and A. Bauen, "Micro-algae cultivation for biofuels: Cost, energy balance, environmental impacts and future prospects," *Biomass and Bioenergy*, vol. 53, pp. 29–38, Jun. 2013, doi: 10.1016/j.biombioe.2012.12.019.

[3] B. Hernández-Carlos and M. M. Gamboa-Angulo, "Metabolites from freshwater aquatic microalgae and fungi as potential natural pesticides," *Phytochem. Rev.*, vol. 10, no. 2, pp. 261–286, 2011, doi: 10.1007/s11101-010-9192

[4] L. Gouveia, A. P. Batista, I. Sousa, A. Raymundo, and N. M. Bandarra, *Microalgae in novel food products*, no. January. 2009.

[5] professor of H. at the U. of T. R. in O. Edwards, Mark Ingeneer Dr. Teruo Higa, *Green Algae Strategy: End Oil Imports And Engineer Sustainable Food And Fuel*. .

[6] M. A. B. Habib, M. Parvin, T. C. Huntington, and M. R. Hasan, *A review of culture, production and use of Spirulina as food for humans and feeds for domestic animals and fish*, no. 1034. 2008.

[7] J. Benemann, "Microalgae for biofuels and animal feeds," *Energies*, vol. 6, no. 11, pp. 5869–5886, 2013, doi: 10.3390/en6115869.

[8] M. Rizwan, G. Mujtaba, S. A. Memon, K. Lee, and N. Rashid, "Exploring the potential of microalgae for new biotechnology applications and beyond: A review," *Renewable and Sustainable Energy Reviews*, vol. 92. pp. 394–404, 2018, doi: 10.1016/j.rser.2018.04.034.

[9] International Energy Agency (IEA), "Market Report Series Renewables 2018 Analysis and Forecast to 2023," *Int. Energy Agency*, p. 211, 2018, [Online]. Available: https://www.iea.org/reports/renewables-2018.

[10] L. Brennan and P. Owende, "Biofuels from microalgae-A review of technologies for production, processing, and extractions of biofuels and co-products," *Renew. Sustain. Energy Rev.*, vol. 14, no. 2, pp. 557–577, 2010, doi: 10.1016/j.rser.2009.10.009.

[11] W. Levasseur, P. Perré, and V. Pozzobon, "A review of high value-added molecules production by microalgae in light of the classification," *Biotechnology Advances*, vol. 41. Elsevier Inc., p. 107545, Jul. 01, 2020, doi: 10.1016/j.biotechadv.2020.107545.

[12] F. Camacho, A. Macedo, and F. Malcata, "Potential industrial applications and commercialization of microalgae in the functional food and feed industries: A short review," *Mar. Drugs*, vol. 17, no. 6, pp. 1–32, 2019, doi: 10.3390/md17060312.

[13] N. Kaur, V. Chugh, and A. K. Gupta, "Essential fatty acids as functional components of foods-a review," doi: 10.1007/s13197-012-0677-0.

[14] M. Dehghani Madvar, A. Aslani, M. H. Ahmadi, and N. S. Karbalaie Ghomi, "Current status and future forecasting of biofuels technology development," *Int. J. Energy Res.*, vol. 43, no. 3, pp. 1142–1160, 2019, doi: 10.1002/er.4344.

[15] F. Alam, S. Mobin, and H. Chowdhury, "Third generation biofuel from Algae," *Procedia Eng.*, vol. 105, no. Icte 2014, pp. 763–768, 2015, doi: 10.1016/j.proeng.2015.05.068.

[16] S. R. Medipally, F. Yusoff, S. Banerjee, and M. Shariff, "Microalgae as Sustainable Renewable Energy Feedstock for Biofuel Production Srikanth.Pdf," vol. 2015, 2015.

[17] E. Kativu, "Carbon Dioxide Absorption Using Fresh Water Algae and Identifying Potential Uses of Algal Biomass," p. 133, 2011.

[18] "ible lipid feedstocks to renewable fuel Ecofuel conversion technology of ined- Microalgae."

[19] J. Masojídek, G. Torzillo, and M. Koblízek, "Photosynthesis in Microalgae," *Handb. Microalgal Cult. Appl. Phycol. Biotechnol. Second Ed.*, no. November 2017, pp. 21–36, 2013, doi: 10.1002/9781118567166.ch2.

[20] A. Alaswad, M. Dassisti, T. Prescott, and A. G. Olabi, "Technologies and developments of third generation biofuel production," *Renew. Sustain. Energy Rev.*, vol. 51, pp. 1446–1460, 2015, doi: 10.1016/j.rser.2015.07.058.

[21] G. C. Zittelli, N. Biondi, L. Rodolfi, and M. R. Tredici, "Photobioreactors for Mass Production of Microalgae," 2013.

[22] Z. Djamal, A. Henni, A. M. Negm, and D. Z. View, "Application of Microalgae in Wastewater Treatment," *Appl. Microalgae Wastewater Treat.*, no. May 2020, 2019, doi: 10.1007/978-3-030-13913-1.

[23] B. Xu, P. Li, and P. Waller, "Study of the flow mixing in a novel ARID raceway for algae production," *Renew. Energy*, vol. 62, pp. 249–257, 2014, doi: 10.1016/j.renene.2013.06.049.

[24] X. Zhang, "Microalgae removal of CO 2 from flue gas flue gas," no. April, 2015.

[25] M. I. Khan, J. H. Shin, and J. D. Kim, "The promising future of microalgae: Current status, challenges, and optimization of a sustainable and renewable industry for biofuels, feed, and other products," *Microb. Cell Fact.*, vol. 17, no. 1, pp. 1–21, 2018, doi: 10.1186/s12934-018-0879-x.

[26] B. Brzychczyk, T. Hebda, J. Fitas, and J. Giełżecki, "The follow-up photobioreactor illumination system for the cultivation of photosynthetic microorganisms," *Energies*, vol. 13, no. 5, 2020, doi: 10.3390/en13051143.

[27] V. Belohlav, T. Zakova, T. Jirout, and L. Kratky, "Effect of hydrodynamics on the formation and removal of microalgal biofilm in photobioreactors," *Biosyst. Eng.*, vol. 200, pp. 315–327, 2020, doi: 10.1016/j.biosystemseng.2020.10.014.

[28] B. L. Gatamaneni, V. Orsat, and M. Lefsrud, “Factors Affecting Growth of Various Microalgal Species,” *Environ. Eng. Sci.*, vol. 35, no. 10, pp. 1037–1048, 2018, doi: 10.1089/ees.2017.0521.
[29] M. Al-Qasmi, N. Raut, S. Talebi, S. Al-Rajhi, and T. Al-Barwani, “A review of effect of light on microalgae growth,” *Lect. Notes Eng. Comput. Sci.*, vol. 2197, no. July, pp. 608–610, 2012.
[30] E. S. Shuba and D. Kifle, “Microalgae to biofuels: ‘Promising’ alternative and renewable energy, review,” *Renew. Sustain. Energy Rev.*, vol. 81, no. April 2016, pp. 743–755, 2018, doi: 10.1016/j.rser.2017.08.042.
[31] J. García *et al.*, “Nutrient removal from agricultural run-o ff in demonstrative full scale tubular photobioreactors for microalgae growth,” no. March, 2018.
[32] J. H. De Vree, *Outdoor microalgae production*. .
[33] L. Xu, P. J. Weathers, X. R. Xiong, and C. Z. Liu, “Microalgal bioreactors: Challenges and opportunities,” *Eng. Life Sci.*, vol. 9, no. 3, pp. 178–189, 2009, doi: 10.1002/elsc.200800111.
[34] C. Wang and C. Q. Lan, “Effects of shear stress on microalgae-A review,” 2018, doi: 10.1016/j.biotechadv.2018.03.001.
[35] A. Ghanem, T. Lemenand, D. Della Valle, and H. Peerhossaini, “Static mixers: Mechanisms, applications, and characterization methods - A review,” *Chem. Eng. Res. Des.*, vol. 92, no. 2, pp. 205–228, 2014, doi: 10.1016/j.cherd.2013.07.013.
[36] S. Soman, “Study of effects of design modification in static mixer geometry and its applications,” *Univ. Waterloo*, 2016.
[37] Noritake, “Helical static mixer.” https://www.noritake.co.jp/eng/products/eeg/middles/detail/.
[38] Sulzer, “Wavy static mixer.” https://www.sulzer.com/en/shared/products/static-mixer.
[39] Chemineer, “HEV Mixers.” https://www.chemineer.com/products/kenics/hev-mixers.html.
[40] J. Ruiz *et al.*, “Towards industrial products from microalgae,” *Energy Environ. Sci.*, vol. 9, no. 10, pp. 3036–3043, 2016, doi: 10.1039/c6ee01493c.
[41] S. Maulana, *An Introduction to Computational Fluid Dynamics THE FINITE VOLUME METHOD*, vol. 2, no. 2. 2016.
[42] “Peristaltic pump, working principles.” https://en.wikipedia.org/wiki/Peristaltic_pump.
[43] Ansys, “ANSYS FLUENT 12.0 Theory Guide - Turbulence.” https://www.afs.enea.it/project/neptunius/docs/fluent/html/th/node42.htm.
[44] C. Clement, “Computational Fluid Dynamics (CFD) Investigation of Hydrodynamic Loading on Subsea Gratings,” no. August, 2016, doi: 10.13140/RG.2.1.4367.6407.
[45] Ansys, “ANSYS FLUENT 12.0 Theory Guide - Standard, RNG, and Realizable k-epsilon Model,” [Online]. Available: https://www.afs.enea.it/project/neptunius/docs/fluent/html/th/node57.htm.
[46] Ansys, “ANSYS FLUENT 12.0 Theory Guide - Boussinesq Approach.” https://www.afs.enea.it/project/neptunius/docs/fluent/html/th/node47.htm.
[47] engineering.com, “Turbulence model,” *engineering.com*. https://www.engineering.com/the-right-turbulence-model-for-your-cfd-simulation.
[48] J. Bardina, P. Huang, and T. Coakley, “Turbulence Modeling Validation, Testing, and Development,” 1997.
[49] Ansys, “ANSYS FLUENT 12.0 training material.” https://www.afs.enea.it/project/neptunius/docs/fluent/html/wbtg/node10.htm.
[50] H. S. Fogler, “Distributions of residence times for chemical reactors,” *Elem. Chem. React. Eng.*, pp. 867–944, 2006.
[51] H. S. Fogler, *Chemical reaction engineering*. 2004.
[52] cadfem, “Boundary-Layer Modeling using Inflation Layers.” https://www.cadfem.in/blog/modeling-boundary-layer-inflation/.
[53] M. Al Hattab, A. Ghaly, and A. Hammouda, “Microalgae Harvesting Methods for Industrial Production of Biodiesel : Critical Review and Comparative Analysis Fundamentals of Renewable Energy and Applications,” *J. Fundam. Rnewable Energy Appl.*, vol. 5, no. 2, pp. 1–26, 2015, doi: 10.4172/20904541.1000154.
[54] Ansys, “ANSYS FLUENT 12.0 Theory Guide - Turbulent Reynolds Number (Re_y).” https://www.afs.enea.it/project/neptunius/docs/fluent/html/ug/node984.htm.
[55] Ansys, “ANSYS FLUENT 12.0 Theory Guide - Postprocessing for Turbulent Flows,” [Online]. Available: https://www.afs.enea.it/project/neptunius/docs/fluent/html/ug/node460.htm.
[56] Ansys, “ANSYS FLUENT 12.0 Theory Guide - Solution and Convergence Criteria.” https://www.afs.enea.it/project/neptunius/docs/fluent/html/tg/node21.htm.

APPENDIX

Assembly drawing (Scale 1:10)

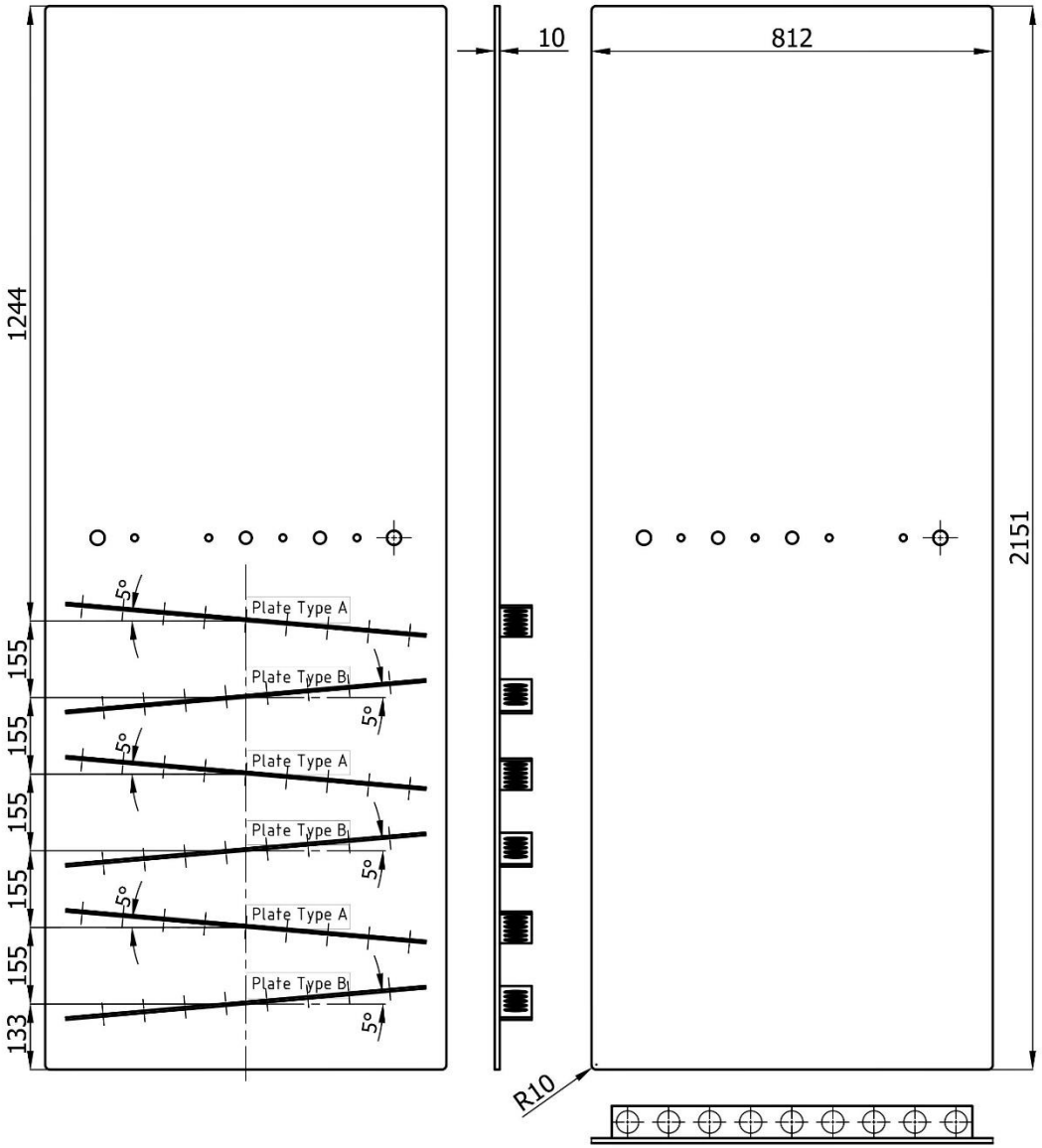

Plate Type A (Scale 1:5)

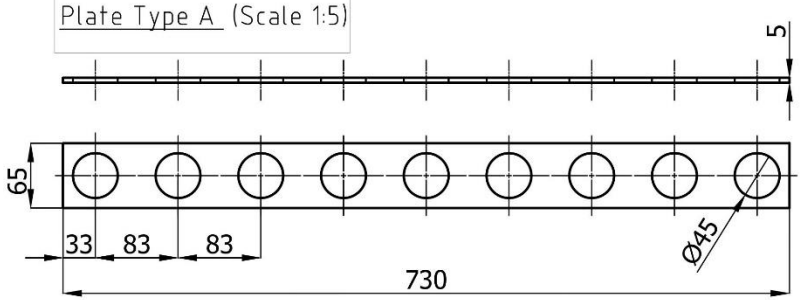

Plate Type B (Scale 1:5)

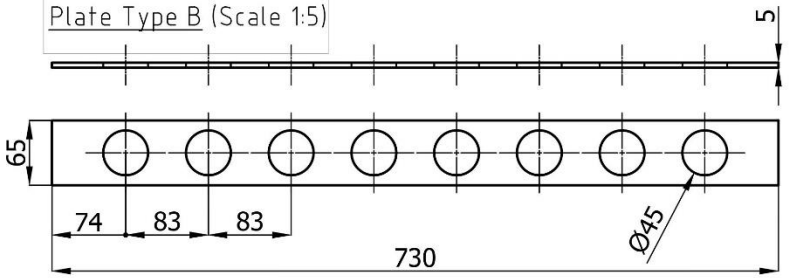

Notes

Two different types of plate will be glued on the flat panel front surface (interior side).
From the top will be installed first plate type A and then B in alternate way.
Each type of plate has a different mounting angle. (See the drawing)

PART LIST

PART	QT	NAME	NOTE
1	3	Plate Type A	N° 9 Holes on 5 mm thick plate
2	3	Plate Type B	N° 8 Holes on 5 mm thick plate
3	1	Front panel	-

PROJECTION: [ISO E] | Unit: mm | A3

CZECH TECHNICAL UNIVERSITY IN PRAGUE
FACULTY OF MECHANICAL ENGINEERING

Customize Front Panel FP PBR

TITLE: IPPsys45_5d_v2

Notes: Integrated front panel with static mixing system.
Inclined Perforated Plates system (IPPs) configuration to avoid sedimentation and increase the light transfer.

Date: 09/02/21

Supervisor: Ing. Mgr. Vojtèch Bèlohlav

Vers: 2.0

Author: Ing. Davide Roletto

Signature

TAV: 1/1

Scale: X